Ticks and Tick-borne Diseases 17 (2026) 102645

Contents lists available at ScienceDirect

Ticks and Tick-borne Diseases

journal homepage: www.elsevier.com/locate/ttbdis

Original article

Metabolomic insights into Lyme neuroborreliosis: Exploring cerebrospinal fluid for diagnostic clues

Ilari Kuukkanen [a,b,*], Annukka Pietikäinen [b,c,d], Tiia Rissanen [e], Saija Hurme [e], Elisa Kortela [f], Jukka Hytönen [b,c,d,1], Maarit Karonen [a,b,1]

[a] Department of Chemistry, University of Turku, Turku, Finland
[b] TBD Turku, University of Turku, Turku, Finland
[c] Institute of Biomedicine, University of Turku, Turku, Finland
[d] TYKS Laboratories, Clinical Microbiology, Turku University Hospital, Turku, Finland
[e] Department of Biostatistics, University of Turku and Turku University Hospital, Turku, Finland
[f] HUS Inflammation Center, Helsinki, Finland

ARTICLE INFO

Keywords:
Borrelia burgdorferi sensu lato
Diagnostic biomarkers, Lyme borreliosis
Lyme neuroborreliosis
Cerebrospinal fluid metabolomics
Tick-borne diseases
UHPLC-MS/MS

ABSTRACT

Lyme neuroborreliosis (LNB), a disseminated manifestation of Lyme borreliosis (LB), arises when *Borrelia burgdorferi* sensu lato (Bbsl) spirochetes disseminate within the host and damage the peripheral nervous system and meninges, and in rare cases, also the parenchyma of the central nervous system (CNS). While early-stage LB is diagnosed clinically, accurate diagnosis of LNB requires cerebrospinal fluid (CSF) analysis, demonstrating pleocytosis and intrathecal synthesis of Bbsl-specific antibodies. There are, however, limitations in current LNB diagnostics, such as the unspecific nature of pleocytosis and post-treatment persistence of intrathecal antibodies necessitating the search for novel biomarkers.

In this study, we employed untargeted ultrahigh-performance liquid chromatography coupled with tandem mass spectrometry (UHPLC-MS/MS) to profile small metabolites (<1500 Da) in CSF samples from subjects with definite acute LNB. Comparative analyses of metabolite profiles were performed between pretreatment subject samples (n = 63) and the following groups: (**A**) a subset of samples collected three weeks after treatment initiation from the same individuals (n = 36), (**B**) Bbsl antibody-negative subjects (non-LNB, n = 61), (**C**) subjects with other CNS infections (n = 21). Additionally, pretreatment LNB samples were compared between individuals with radiculitis (n = 40) and those without radiculitis (n = 23) (**D**).

Out of 4222 molecular features (MFs) detected, 131 were prioritized based on statistical significance and magnitude of change for further detailed structural characterization. Altered metabolite classes included compounds from lysophospholipids [e.g., lysophosphatidylcholine (16:0), and lysophosphatidylethanolamine (18:0)], sphingomyelins [e.g., sphingomyelin (d18:1/14:0) and sphingomyelin d16:1/16:0)], sphingoid bases (e.g., d19:0 sphinganine, and 3-ketosphingosine), fatty acid amides (e.g., palmitoleamide and oleamide), cyclic phosphatidic acids [i.e., cyclic phosphatidic acid (16:0) and cyclic phosphatidic acid (18:2)], and amino acid metabolism (i.e., DL-glutamine, 5-hydroxytryptophan and DL-kynurenine).

These findings underscore the potential of CSF metabolomics as a powerful complementary tool for diagnosing LNB and differentiating it from other CNS conditions. The identified metabolic signatures offer a foundation for future biomarker development and may enhance diagnostic precision, guide treatment strategies, and deepen our understanding of LNB pathogenesis.

1. Introduction

Lyme neuroborreliosis (LNB) is a disseminated manifestation of Lyme borreliosis (LB), the most prevalent tick-borne zoonotic disease in Europe and North America. LB is caused by spirochetes of the *Borrelia burgdorferi* sensu lato (hereafter referred to as Bbsl) complex and is

* Corresponding author.
E-mail address: ilari.j.kuukkanen@utu.fi (I. Kuukkanen).
[1] These authors contributed equally to this work.

https://doi.org/10.1016/j.ttbdis.2026.102645
Received 15 December 2025; Received in revised form 6 April 2026; Accepted 12 April 2026
Available online 18 April 2026

transmitted through the bite of Bbsl-infected ticks of the genus *Ixodes* (Steere et al., 2016). In LNB, Bbsl affects the nervous system, typically within a few weeks of exposure (Koedel et al., 2015; Stanek et al., 2011).

Early LB is commonly characterized by an expanding skin lesion known as erythema migrans, marking the localized infection phase. In contrast, early disseminated LNB can present neurological signs such as lymphocytic meningitis, cranial neuropathies and radiculitis, collectively referred to as Garin-Bujadoux-Bannwarth syndrome (Steere et al., 2016). While erythema migrans is primarily diagnosed clinically, disseminated forms require laboratory confirmation. Serological detection of Bbsl-specific antibodies in serum and cerebrospinal fluid (CSF) remains the cornerstone of LB and LNB diagnostics (Branda and Steere, 2021; Kullberg et al., 2020). A definitive diagnosis of LNB requires evidence of CSF pleocytosis, demonstration of intrathecal synthesis of Bbsl-specific antibodies, and the presence of compatible neurological symptoms (Branda and Steere, 2021; Kullberg et al., 2020; Mygland et al., 2010). However, antibodies may take several weeks to develop before being detectable in CSF, and on the other hand, serological tests have limited utility in distinguishing active infection from past episodes, as subjects may remain seropositive long after resolution of the disease (Hammers-Berggren et al., 1993; Kalish et al., 2001). Additionally, false-positive results due to cross-reactive antibodies from other infections can occur (Grąźlewska and Holec-Gąsior, 2023; Wojciechowska-Koszko et al., 2022). Thus, additional biomarkers are needed to overcome the diagnostic and follow-up limitations of current LNB laboratory methods.

CXCL13 (C-X-C motif chemokine ligand 13) has emerged as a promising CSF biomarker for acute, untreated LNB (Hytönen et al., 2014; Pietikäinen et al., 2018; Waiß et al., 2024). This chemokine directs B-cell migration and rises rapidly during early infection, preceding Bbsl-specific antibody responses, and declines promptly after effective antimicrobial treatment (Cyster et al., 2000; Gunn et al., 1998; Rupprecht et al., 2008; Schmidt et al., 2011). These dynamics make CXCL13 a valuable early indicator when serology is inconclusive. However, CXCL13 lacks disease specificity and should be interpreted alongside other diagnostic criteria (Smíšková et al., 2023).

In this study, we applied metabolomics based ultrahigh-performance liquid chromatography (UHPLC) integrated with tandem mass spectrometry (MS/MS). This high-throughput analytical approach aimed at detecting and identifying small metabolites (<1500 Da), in CSF samples from acute definite LNB subjects (pretreatment and three weeks after antibiotic treatment initiation), age- and sex-matched non-LNB control subjects, and from subjects with other CNS infections. We aimed to identify LNB-specific CSF metabolite signatures that provide improved diagnostic precision and facilitate differentiation between subject groups.

2. Materials and methods

2.1. Chemicals

Analytical grade ethanol and methanol, as well as LC-MS grade formic acid, were procured from VWR International (Fontenay-Sous-Bois, Paris, France). LC-MS grade acetonitrile was supplied by Fisher Scientific (Loughborough, Leicestershire, United Kingdom). Deuterated standards, including DL-phenyl-d_5-alanine and L-tryptophan-(indole-d_5), were obtained from Cambridge Isotope Laboratories Inc. (Andover, Massachusetts, USA). Reference standards acetyl-DL-carnitine, LysoPC (15:0), LysoPC(17:0), LysoPC(18:1), DL-kynurenine were ordered from Sigma-Aldrich International GmbH (Buchs, Switzerland). Additionally, (*R*)-2-hydroxy-3-(palmitoyloxy)propyl (2-(trimethylammonio)ethyl) phosphate and (2S,3R, E)-3-hydroxy-2-palmitamido-octadec-4-en-1-yl (2-(trimethylammonio)ethyl) phosphate were purchased from BLD Pharmatech GmbH (Reinbek, Germany). Ultra-pure type I water was generated using a Merck Millipore Synergy UV system.

2.2. Cerebrospinal fluid samples

The definite acute LNB subject group CSF samples were originally collected, along with their serum sample counterparts, as part of our previously published LNB treatment study, which compared the treatment outcomes of intravenous ceftriaxone and oral doxycycline in LNB (Kortela et al., 2021). In the present study, we analyzed CSF samples from the subjects, who had been classified as definite acute LNB, following the European Federation of Neurological Societies (EFNS) criteria (Mygland et al., 2010). CSF samples from 63 individual subjects were available for this study. These samples were collected at diagnosis, prior to the initiation of the antibiotic treatment. Among the definitive LNB subjects there were 19 female (30%) and 44 male subjects (70%). The median age of LNB subjects was 58 years (range: 18 to 79 years). Radiculitis was present in 40 subjects and absent in 23. More detailed subject characteristics are provided in Table 1. Additionally, in a subgroup of subjects (n = 36), a CSF sample was collected three weeks after treatment initiation for those with ≥50 leukocytes/μL in the pretreatment CSF sample, as specified in the original study protocol (Kortela et al., 2021). Of these, 22 subjects received oral doxycycline, while 14 were treated with intravenous ceftriaxone.

All control subject group samples were collected as part of routine diagnostic procedures prior to initiation of treatment. Non-LNB CSF samples (n = 61; age- and sex-matched to LNB subjects) were collected from subjects clinically suspected of having LNB, but who were without detectable intrathecal Bbsl-specific antibody production, and who were also Bbsl antibody-negative in the serum using an in-house whole cell antigen preparation-based EIA test (Viljanen and Punnonen, 1989). Two subjects with acute LNB did not have corresponding non-LNB controls available for comparison.

CSF pretreatment samples from subjects with other laboratory diagnosed CNS infections (n = 21) were also included: tick-borne encephalitis (TBE, n = 9), Herpes simplex virus (HSV, n = 6) and Varicella zoster virus (VZV, n = 6). The TBE samples were IgM positive in CSF and IgM and IgG positive in serum (n = 6), TBE IgM positive in CSF only (n = 1) or TBE IgM and IgG positive in serum (n = 2) as analyzed by an enzyme-linked immunosorbent assay (Reagena, Toivala, Finland). The HSV and VZV CSF samples were PCR positive (in house PCR assays). After the sample collection, all clinical CSF were stored at −20 °C in freezers without an automatic frost-free cycle.

All individuals participating in the LNB treatment study had provided an informed consent, and ethical approval was granted by the National Committee on Medical Research Ethics in Finland. The present study adhered to the ethical principles of the Declaration of Helsinki for research involving human material and data. All samples were coded to ensure subject anonymity. Permission for the study was obtained from the Health District of South-Western Finland (Permission No T012/004/19).

2.3. Sample preparation and analytical workflow

The sample preparation protocol was adapted from our previous study (Kuukkanen et al., 2025). For this study, the available CSF sample volume was 50 μL. As the original protocol was optimized for 150 μL of serum, proportional adjustments were made to reagent volumes and pretreatment steps to ensure compatibility with the lower CSF sample volume. All processing steps, including macromolecule precipitation, were scaled accordingly while maintaining the relative ratios of solvents and internal standards to preserve analytical consistency across samples.

2.4. UHPLC-QOrbitrap-MS/MS analysis, in silico metabolomics, molecular feature identification and metabolic set enrichment analysis

UHPLC-QOrbitrap-MS/MS analysis, *in silico* metabolomics, and molecular feature (MF) detection from the raw data, together with data standardization using internal standards and the estimated use of

Table 1
Baseline subject characteristics from cerebrospinal fluid (CSF) samples, by subject group. The study comprised four groups: definite acute pretreatment Lyme neuroborreliosis (LNB); LNB three weeks after initiation of antibiotic treatment (same individuals as the pretreatment LNB subgroup); *Borrelia burgdorferi* sensu lato antibody-negative (non-LNB) controls matched by age and sex to LNB subjects; and other central nervous system (CNS) infections: tick-borne encephalitis (TBE), Herpes simplex virus (HSV), and Varicella zoster virus (VZV). For LNB subgroups, antibiotic treatment is reported by route (intravenous ceftriaxone or oral doxycycline). For LNB subjects, CSF leukocyte counts and C-X-C motif chemokine ligand 13 (CXCL13) concentrations were available. Radiculitis indicates presence/absence among pretreatment LNB subjects. CSF was collected before treatment for all groups except the LNB three weeks after initiation of antibiotic treatment subgroup. Categorical variables are reported as n (%) or continuous variables as median (range).

Subject characteristics		Subject group															
		LNB, pretreatment				LNB, three weeks◊				Non-LNB				Other CNS infections			
		Female (n = 19)		Male (n = 44)		Female (n = 13)		Male (n = 23)		Female (n = 18)		Male (n = 43)		Female (n = 10)		Male (n = 11)	
	Age*	61	(18 - 75)	52	(28 - 79)	61	(31 - 75)	55	(28 - 78)	62	(18 - 74)	52	(28 - 79)	62	(31 - 90)	62	(18 - 79)
Antibiotic treatment	Ceftriaxone**	6	(33%) ****	24	(55%) ****	4	(31%)	10	(44%)	-	-	-	-				
	Doxycycline***	13	(68%) ****	20	(46%) ****	9	(69%)	13	(57%)	-	-	-	-				
CSF	Leukocytes [cells×ml^{-1}]*	204	(5 - 530)	80	(7 - 985)	56	(11 - 92)	34	(0 - 147)	-	-	-	-				
	CXCL13* [pg×ml^{-1}]	3400	(0 - 42,364)	4517	(0 - 675,000)	109	(7 - 318)	122	(7 - 1830)	-	-	-	-				
CNS infection	TBE	-	-	-	-	-	-	3	(30%)	6	(55%)						
	HSV	-	-	-	-	-	-	4	(40%)	2	(18%)						
	VZV	-	-	-	-	-	-	3	(30%)	3	(27%)						
Radiculitis	No	4	(21%)	19	(43%)	-	-	-	-	-	-						
	Yes	15	(79%)	25	(57%)	-	-	-	-	-	-						

Values are presented as counts and percentages, n (%) for categorical variables. Median with range was reported for continuous variables due to the violation of normality assumption.
◊ CSF samples obtained from the same individuals within the pretreatment LNB subgroup, *Median (range), **Intravenous administration, ***Oral administration, ****At the time of diagnosis, patients in the acute pretreatment phase of LNB had not yet received antibiotic treatment, - Data not available.

acetaminophen (APAP), based on the detection of APAP and its metabolites in the MS data, were conducted as previously described (Kuukkanen et al., 2025). MF classification followed the same criteria (Kuukkanen et al., 2025) and MF identifications were assigned using the five-level system (Schymanski et al., 2014), based on the Metabolomics Standards Initiative (MSI) framework for minimum reporting standards in metabolomics (Sumner et al., 2007). In this system, **Level 1** represents confirmed structural identification using a reference standard; **Level 2** corresponds to tentative annotation based on MS/MS spectral matching with literature or databases; **Level 3** indicates a tentative candidate structure supported by molecular formula and fragment information; **Level 4** reflects features assigned only with a molecular formula (including isotopic pattern, adduct formation, and charge state); and **Level 5** is an unclassified, yet distinct, mass spectral feature.

To better understand the connections associated with the observed metabolomic and molecular pathway changes, a metabolomic set enrichment (MSE) pathway analysis (Lu et al., 2023) was performed with MetaboAnalyst platform version 6.0 (Pang et al., 2024), utilizing Relational database of Metabolomic Pathways (RaMP-DB) for metabolite and lipid pathways (Braisted et al., 2023), which is integrated with Kyoto Encyclopedia of Genes and Genome (Kanehisa et al., 2025) via Human Metabolome Database (HMDB) (Wishart et al., 2022), REactome (Jassal et al., 2019) and WikiPathways (Slenter et al., 2018). RaMP-DB metabolite sets containing at least three entries were required. The MSE analysis was done for the selected subset of the most prominent and well characterized features with positive HMDB identifications.

2.5. Statistical analysis

Statistical analyses were performed across three main comparisons separately: (**A**) between pretreatment LNB CSF samples and three weeks after treatment initiation LNB CSF samples, (**B**) between pretreatment LNB CSF samples and age- and sex-matched non-LNB control samples, (**C**) between pretreatment LNB CSF samples and CSF samples representing other CNS infections. Comparisons **A** and **B** involved paired observations and were therefore conducted using the Wilcoxon signed rank test. Comparison **C** was based on independent samples and was evaluated using the Wilcoxon rank sum test. Due to the non-normality of the distributions, non-parametric methods were applied.

Differences were examined in all MFs. The MFs which were statistically significant (level set at 0.001) in both datasets (raw and standardized) were examined more closely and visualized with volcano plots. For these most significant MFs multivariable models were conducted to evaluate the effects of patients' characteristics. Linear mixed models for repeated measures were performed in comparisons **A** and **B** using compound symmetry covariance structure. Logarithmic transformations were used to achieve the normal distribution assumption of MFs. In comparison **A**, models included one within-factor (timepoint: pretreatment, three-week after) and several between factors (age, sex, CSF leukocyte count, use of APAP, CFS CXCL13 concentration). In comparison **B**, models included one within-factor (matched pair: pretreatment sample and age- and sex-matched controls) and three between factors (age, sex, use of APAP). Linear regression models were used in comparison **C** and models included three explanatory variables (age, sex, use of APAP).

Additionally, subgroup analysis was performed to compare CSF samples of pretreatment LNB subjects with and without radiculitis (comparison **D**). The differences between LNB subjects with and without radiculitis in all MFs were studied with the same analysis methods as in comparison **C**.

The normality of variables was evaluated visually and tested with the Shapiro-Wilk test. Tests were performed as two-sided with a significance level set at 0.05. The analyses were carried out using the RStudio (version 2024.09.1 Build 394) based on R (version 4.4.3; RStudio, PBC, Boston, MA, USA).

3. Results

A total of 4222 MFs were detected across the CSF samples. In comparisons **A, B** and **C**, the statistically most significant MFs ($p < 0.001$)

were selected for further evaluation. In comparison **D**, a significance threshold of $p < 0.05$ was applied. Linear mixed models were applied to assess the impact of subject characteristics on individual MFs ($p < 0.05$), including subject group, age, sex, treatment center, CSF leukocyte count, CSF CXCL13 concentration, and APAP use based on the detection of APAP and its metabolites in the MS data. Not all subject-specific variables were available for all four comparisons **A**-**D**. An overview of the integrated workflow is presented in Fig. 1.

Selected MFs were further filtered based on effect magnitude, with a threshold of five-fold median change and a median difference in peak area exceeding 5×10^5 (counts × seconds). In comparison **D**, a more permissive threshold ($p < 0.05$) was used, along with a three-fold median change and a minimum peak area difference of 3×10^5 (counts × seconds). Applying these criteria, 131 MFs were prioritized for structural characterization (**Supplementary Table S1**). Distribution of the prominent MFs across the comparisons is detailed in **Supplementary Table S2**.

3.1. *Comparison A: CSF samples collected before LNB treatment and three weeks after treatment initiation*

Pairwise statistical comparison (n = 36) identified 977 MFs with statistically significant differences ($p < 0.001$) when comparing pretreatment CSF samples from subjects with acute LNB to their respective samples collected three weeks after treatment initiation. Of these, 60 MFs were selected for further evaluation based on sustained statistical significance after adjustment for relevant subject characteristics, including subject group, age, sex, CSF leukocyte count, CXCL13 concentration, and use of APAP. Structural characterization and removal of molecular replicates following *in silico* metabolomic analysis resulted in 52 MFs, including seven MFs derived from medication. These features, showing both upregulated and downregulated metabolites, are presented in the volcano plot (Fig. 2A) and in the heatmap (Fig. 3A). Detailed MF annotations are available in **Supplementary Table S1.**

No single MF was influenced by all selected variables. Analysis of estimated subject group effect, comparing pretreatment LNB subjects with those treated with either oral doxycycline or intravenous ceftriaxone, revealed significant differences in 15 MFs. Doxycycline (MF2938), an in-source MS fragment ion of doxycycline (MF2978), and a metabolic product of doxycycline (MF2235) were excluded from the analysis because doxycycline was strongly upregulated among the three weeks after treatment initiation samples. Aside from these excluded MFs, no statistically significant overall effect of doxycycline was observed among the remaining MFs in comparison **A**. Ceftriaxone was not among the significant MFs. The median estimated subject group effect across included features was 71.03% (range: 1.01% to 92.44%) higher among the pretreatment LNB subject samples. Notably, subject group alone did not independently account for variation in any MF.

Subject age significantly influenced 40 MFs, with a median estimated effect of 5.66% (range: 1.59% to 14.75%). Age alone accounted for the variation in 14 of these features. The most pronounced age-associated effects were observed in lipophilic compounds eluting at later retention times.

Subject sex had a statistically significant effect on five MFs, with a median estimated effect of –51.53% (range:51.53% to –85.56%) in males compared to females. This finding suggests a potential sex-specific influence in the regulation or expression of these features. Among them, age alone accounted for the variation in one MF (MF3545), with a notable estimated effect of –85.56%.

CXCL13, a cerebrospinal fluid biomarker for LNB and an established diagnostic marker (Hytönen et al., 2014; Waiß et al., 2024), modeled as a continuous variable, significantly influenced 19 MFs. One of these features, (MF1437), identified as a sodium adduct ion of APAP-glucuronide, was excluded from this group. However, the median estimated effect across models was 0.0064% change in MF per unit increase in CXCL13 (95% CI range: 0.0053% to 0.0071%). Moreover, CXCL13 did not independently explain the variation in any individual MF. Most of these affected features were classified as lipophilic compounds.

Compared to non-users, APAP users (identified from the UHPLC-MS/MS data) exhibited significant alterations in six MFs, with a strong median estimated effect increase of 99.35% (range: 45.11% to 99.91%). Five of these MFs were identified directly as APAP related metabolites (MF1437, MF1441, MF1442, MF1456). One unidentified MF exhibited

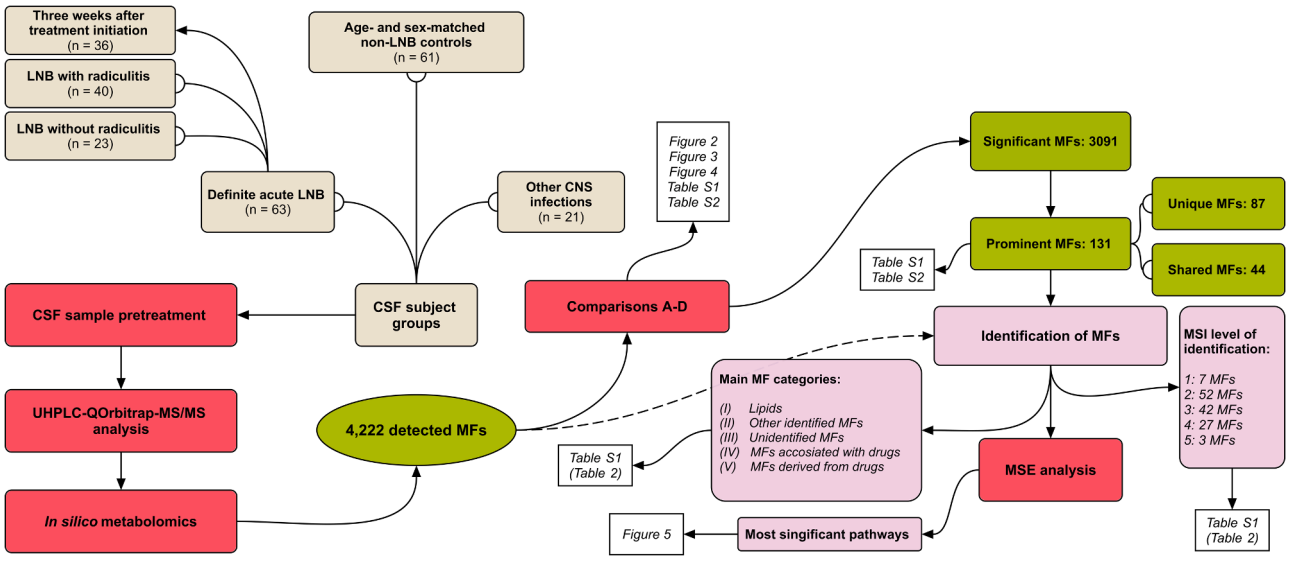

Fig. 1. Integrated workflow of cerebrospinal fluid (CSF) sample processing and molecular feature (MF) analysis across subject groups, including sample pretreatment, ultrahigh-performance liquid chromatography–tandem mass spectrometry (UHPLC–MS/MS) analysis, *in silico* metabolomics with MF detection, statistical comparisons **A**-**D**, subsequent MF identification and classification, and metabolite set enrichment (MSE) analysis, as detailed in the figures (Figs. 2–5) and tables (Table 2 and Supplementary information **Tables S1**-**S2**). The main statistical comparisons comprise: (**A**) paired pretreatment Lyme neuroborreliosis (LNB) samples vs samples collected three weeks after initiation of antibiotic treatment; (**B**) pretreatment LNB samples vs age- and sex-matched *Borrelia burgdorferi* sensu lato antibody-negative (non-LNB) controls; (**C**) pretreatment LNB samples vs CSF from other central nervous system (CNS) infections, including tick-borne encephalitis (TBE), Herpes simplex virus (HSV), and Varicella zoster virus (VZV); and (**D**) pretreatment LNB samples from subjects with vs without radiculitis.

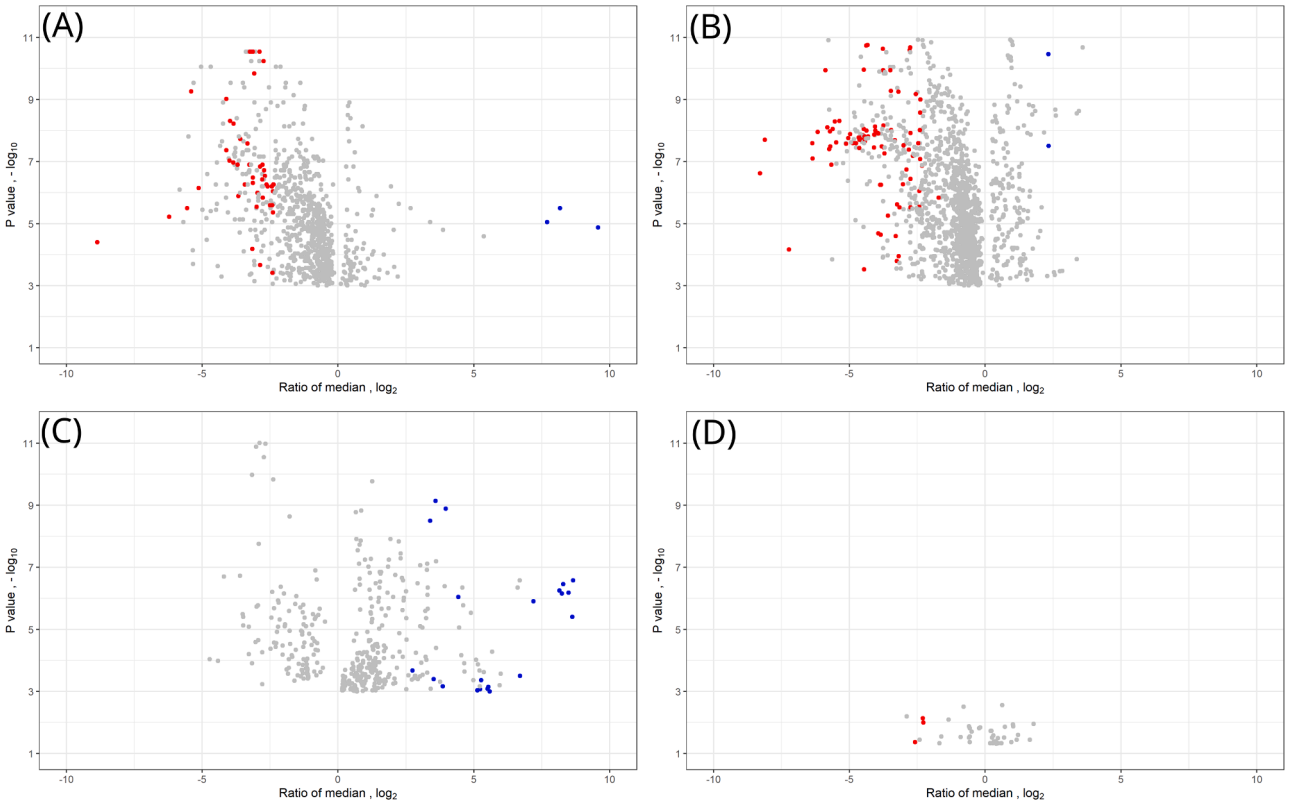

Fig. 2. Volcano plots of most significant molecular feature (MF) median peak areas across the four main comparisons **A-D**. Red color indicates significant decreases in MF peak areas (reflecting reduced MF concentrations), whereas blue indicates significant increases (reflecting elevated MF concentrations). (**A**) comparison A: A total of 977 MFs were significantly altered ($p < 0.001$) between cerebrospinal fluid (CSF) samples from acute Lyme neuroborreliosis (LNB) subjects before antibiotic treatment (reference) and at three weeks after treatment initiation; the 52 most prominent MFs are highlighted. (**B**) comparison B: 1421 MFs differed significantly ($p < 0.001$) between CSF samples from pretreatment LNB subjects (reference) and *Borrelia burgdorferi* sensu lato antibody-negative (non-LNB) controls matched for age and sex; the 87 most prominent MFs are highlighted. (**C**) comparison C: 596 MFs differed significantly ($p < 0.001$) between CSF samples from pretreatment LNB subjects (reference) and those from subjects with other central nervous system (CNS) infections [tick-borne encephalitis (TBE), Herpes simplex virus (HSV) and Varicella zoster virus (VZV)]; the 21 most prominent MFs are highlighted. (**D**) comparison D: 97 MFs differed significantly ($p < 0.05$) between CSF samples from LNB subjects with (reference) and without radiculitis; the three most prominent MFs are highlighted.

an effect of 45.11%.

3.2. Comparison B: CSF samples from pretreatment LNB patients and Bbsl antibody-negative non-LNB controls

A total of 1421 MFs showed statistically significant differences ($p < 0.001$) between CSF samples from subjects with acute LNB to those from age- and sex-matched non-LNB controls, based on 61 pairwise comparisons in the statistical analysis. From these, 94 MFs were selected for further evaluation based on sustained statistical significance, after evaluation of relevant subject characteristics: subject group, sex, and APAP use. Structural characterization and removal of molecular replicates following *in silico* metabolomic analysis resulted in 87 MFs. None of the selected MFs were influenced by all variables included. These features are presented in the volcano plot (Fig. 2B) and in the heatmap (Fig. 3B). Detailed annotations and characterizations are provided in **Supplementary Table S1**.

Based on the pairwise statistical comparison (n = 61), the median estimated subject group effect was –89.13% (range:92.44% to 400.17%) for non-LNB compared to pretreatment LNB subjects. Notably, two features were markedly upregulated among non-LNB subjects: MF749, tentatively identified as DL-glutamine (estimated effect: 306.87%), and MF1690, a potential hypoxanthine derivative (estimated effect: 400.17%). The subject group alone accounted for the variation in 55 MFs.

Subject age was a statistically significant factor for 27 MFs, with a median estimated variable effect of 2.96% (range: 0.95% to 6.73%). Subject sex was significantly associated with four MFs, all classified as lipids, and showed a median estimated variable effect of −67.44% (range: −72.87% to −61.36%) in males compared to females.

Use of APAP was also evaluated and found to significantly affect seven MFs, with a median estimated effect of –36.64% (range:50.92% to –30.03%) in non-LNB subjects compared to pretreatment LNB subjects. None of these seven MFs were identified as APAP, its known metabolites, or related mass spectral fragment or adduct ions. Additionally, these MFs were also affected by the subject group and subject age. It is highly likely that this overlap reflects both disease-related alterations in the metabolomic profile and potential modulation by common medications like APAP.

3.3. Comparison C: CSF samples from pretreatment LNB patients and patients with other CNS infections

Independent statistical comparisons (n = 84) of CSF samples from subjects with acute LNB (n = 63) and those with other laboratory confirmed CNS infections (n = 21) identified 596 MFs with statistically significant differences ($p < 0.001$). To further assess the effect of individual variability, associations between MFs and subject characteristics (group, age, sex, and APAP use) were analyzed. Of 35 MFs, a subset of 21 MFs was selected for detailed investigation based on statistical significance, as well as their median fold change and change in peak area. None of the MFs were affected by all selected study variables. These features are presented in the volcano plot (Fig. 2C) and in the heatmap (Fig. 3C). More detailed characterization for these MFs can be found in

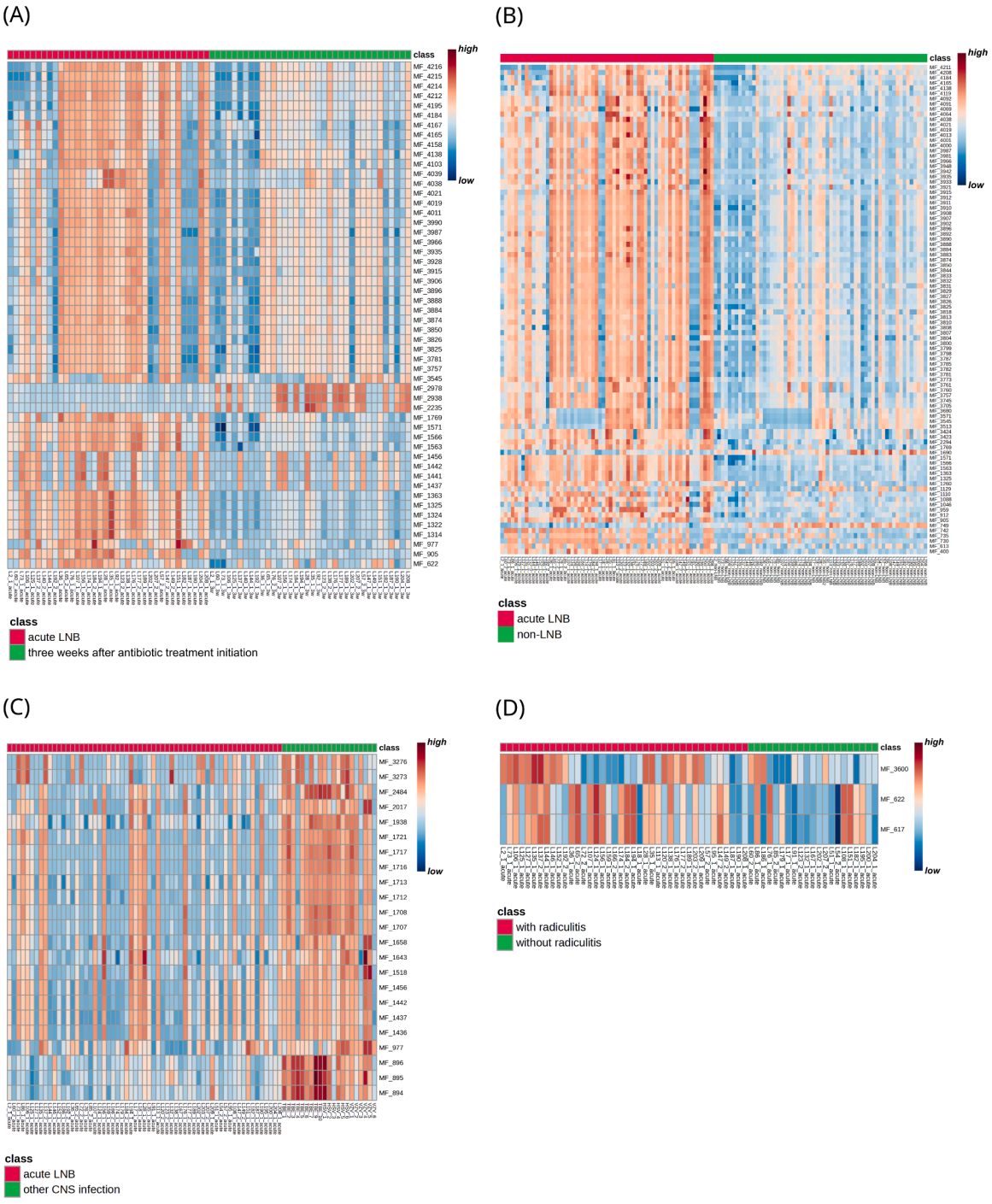

Fig. 3. Heatmap panels of statistically significant molecular feature (MF) peak areas across individual subjects for the main comparisons: (A) paired pretreatment Lyme neuroborreliosis (LNB) samples vs samples collected three weeks after initiation of antibiotic treatment; (B) pretreatment LNB samples vs age- and sex-matched Borrelia burgdorferi sensu lato antibody-negative (non-LNB) controls; (C) pretreatment LNB samples vs cerebrospinal fluid (CSF) samples from other central nervous system (CNS) infections, including tick-borne encephalitis (TBE), Herpes simplex virus (HSV), and Varicella zoster virus (VZV); (D) pretreatment LNB samples from subjects with vs without radiculitis. In each heatmap, the x-axis represents individual CSF samples, with comparison-specific classes indicated at the top according to subject group distribution. The y-axis represents comparison-specific MFs. Standardized peak areas are visualized using a color gradient, where red indicates higher MF peak areas and blue indicates lower peak areas.

Supplementary Table S1.

Comparison between subject groups revealed significant differences in only four MFs, all exclusively influenced by the group. The median estimated group effect was –76.40% (range:77.86% to 716.34%) in subjects with other CNS infections compared to pretreatment LNB. Three of these features appear structurally related and may originate from a common precursor ion, i.e., MF894 (estimated effect:77.86%), tentatively identified as purine nucleoside, and its presumed product ions MF896 (estimated effect:75.76%) and MF895 (estimated effect:77.04%). The fourth MF (MF977) was confirmed using a reference standard as acetylcarnitine, showing an estimated effect 715.34% higher in other CNS infection subjects.

Subject age significantly influenced two MFs in this comparison (excluding five directly APAP-related MFs), with a median estimated

effect of –5.70% (range:6.07% to –5.34%). These features were exclusively affected by age. Subject sex showed no significant association with any of the selected MFs. In contrast, APAP use was associated with changes in 15 MFs, all identified as direct APAP-related metabolites. Among non-users, the median estimated effect was markedly reduced at –99.63% (range:99.95% to –93.51%) compared to identified APAP users. Six MFs remained as prominent biomarkers in this comparison, none of which were medication related.

3.4. Comparison D: Pretreatment LNB CSF samples with and without radiculitis

Independent statistical comparisons (n = 63) were performed between LNB subjects with (n = 40) and without reported radiculitis (n = 23). For this analysis, a significance level of 0.05 was applied, identifying 97 MFs as statistically significant. Further evaluation incorporating relevant subject characteristics: subject group, age, sex, CSF leukocyte count, CXCL13 concentration and estimated APAP use, along with additional filtering criteria of a ≥three-fold median change and a median change exceeding 3×10^5 peak area (counts × seconds), reduced the number of candidates to three. These selected MFs are presented in the volcano plot (Fig. 2D) and in the heatmap (Fig. 3D). Detailed MF characteristics are provided in **Supplementary Table S1**.

Comparison **D** revealed significant associations with all three MFs, showing a strong subject group median estimated effect of 117.63% (range: 102.85% to 329.05%) in subjects with radiculitis compared to those without. However, these features were not exclusively driven by the subject group. Subject age was significantly associated with MF3600, tentatively identified as isopropanolamine myristate, with an estimated effect of –4.37%. CSF leukocyte count (continuous variable) also showed significant associations with MF617 (estimated effect: 0.33%) and MF622 (estimated effect: 0.30%). No significant associations were observed for subject sex, CXCL13 concentration or APAP use.

3.5. Shared and distinct MFs identified across the comparisons A-D

To summarize the results across all four comparisons, we assessed both the overlapping and the unique MFs identified in each analysis. This integrative cross-comparison enabled the detection of MFs exhibiting consistent and robust alterations across the analyzed datasets, while also highlighting unique features specific to individual comparisons.

Among the 4222 detected MFs, 141 prominent non-medication-related MFs were identified across comparisons **A-D**. Fallowing deduplication, 112 non-medication MFs remained (83 unique and 29 shared) as shown in Fig. 4. In addition, 19 statistically significant MFs directly associated with medication were identified. For completeness, when both medication-related and non-medication MFs were considered prior to detailed characterization and statistical evaluation, the combined set comprised 131 MFs, of which 87 were unique and 44 were shared across comparisons **A**–**D**.

None of the 131 MFs (19 directly medication related MFs and 112 non-medication MFs) were shared across all four comparisons. Comparison **A** shared 27 MFs with comparison **B**, one MF with comparison **C**, and one MF with comparison **D**. After excluding features directly linked to medication use (one APAP-related and three doxycycline-related MFs), comparison **A** retained 45 relevant MFs, comprising 16 unique and 29 shared features.

Comparison **B** did not share any MFs with comparisons **C** or **D** and included no features directly attributed to medication use. Consequently, 60 MFs were considered specific to comparison **B**. However, as previously noted, eight of these were significantly influenced by

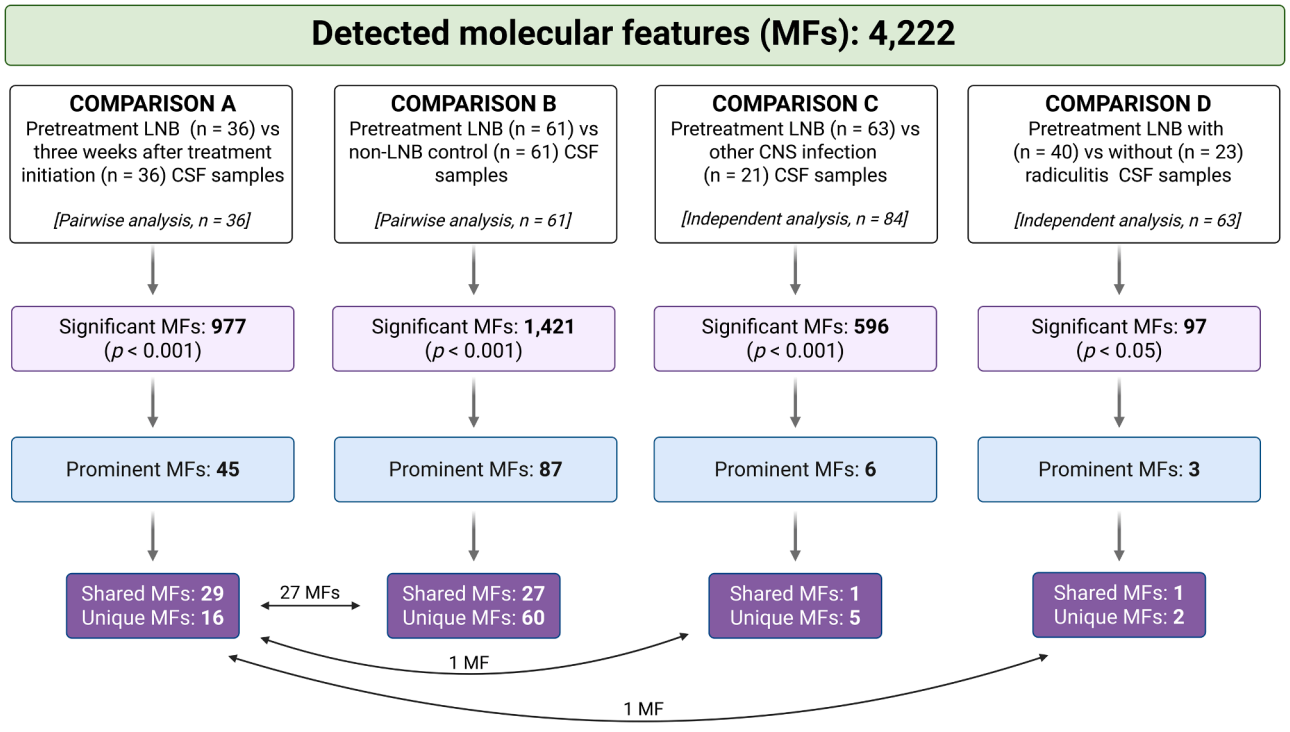

Fig. 4. Cross-comparison of statistically significant non-medication molecular features (MFs) in cerebrospinal fluid (CSF) across comparisons A–D. Comparisons were defined as follows: (A) paired pretreatment Lyme neuroborreliosis (LNB) CSF vs CSF collected three weeks after initiation of antibiotic treatment; (B) paired pretreatment LNB CSF vs age- and sex-matched Borrelia burgdorferi sensu lato antibody-negative (non-LNB) control CSF; (C) pretreatment LNB CSF vs CSF from other central nervous system (CNS) infections; (D) pretreatment LNB CSF from subjects with vs without radiculitis. Among 4222 detected MFs, 141 prominent non-medication candidate MFs were initially prioritized (A: 45; B: 87; C: 6; D: 3). Following deduplication across comparisons, 112 non-medication MFs remained (83 unique and 29 shared), as shown. Directly medication-associated MFs were excluded from the figure. Panels distinguish shared MFs (present in ≥ two comparisons), unique MFs (present in a single comparison), and the most prominent MFs among statistically significant MFs.

estimated APAP use. For comparison **C**, after excluding one MF shared with comparison **A** and 17 features identified as direct APAP metabolites, five MFs remained specific to this comparison. Comparison **D** exhibited one overlapping MF with comparison **A**, leaving two MFs unique to this comparison.

3.6. Metabolite profiling, structural elucidation and enriched pathway changes

Automatic pre-characterization of the 4222 MFs was performed during the *in silico* metabolomic analysis based on the exact mass and, when available, MS/MS spectral data. This resulted in the tentative identification of 1753 MFs, while molecular formulae were successfully assigned to 3897 MFs.

Following statistical evaluation and structural identification, the final 131 MFs were manually examined and characterized based on their exact mass, molecular formula (derived from exact mass), MS/MS spectral patterns, retention time, database matches, statistical properties and behavior, and when possible, comparison with reference standards.

Classification of the 131 MFs was organized into five main categories: (**Category I**) lipids and lipid-type compound MFs (76 MFs); (**Category II**) other identified endogenous or exogenous metabolite MFs (27 MFs); (**Category III**) currently unidentified MFs that may serve as potential biomarkers for LNB (6 MFs); (**Category IV**) MFs statistically associated with medication use or MFs associated with medication use, with infection-related processes contributing to these alterations as well (8 MFs); (**Category V**) MFs directly derived from medication (19 MFs). **Categories II** and **III** shared five MFs that were classified in both categories. Two MFs in **category IV** and four in **category V** could not be assigned a molecular formula based on their exact masses.

Across the final 131 MFs, annotation confidence varied according to the evaluated MSI levels. A total of seven MFs were assigned to MSI **Level 1**, representing confirmed structural identification using authentic reference standards. **Level 2** included 52 MFs, corresponding

Table 2
Representative subset of statistically significant molecular features (MFs) detected in cerebrospinal fluid (CSF). Columns indicate the MF, ion mass and corresponding ion, molecular formula, tentative identification, Metabolomics Standards Initiative (MSI) identification level, and the assigned MF category based on the identification.

Molecular feature	Ion mass	Ion	Molecular formula	Tentative identification	MSI*	Category
MF3825	496.33968	$[M+H]^+$	$C_{24}H_{50}NO_7P$	LysoPC(16:0)	1	I
MF3910	522.35571	$[M+H]^+$	$C_{26}H_{52}NO_7P$	LysoPC(18:1)	1	I
MF4215	703.57445	$[M+H]^+$	$C_{39}H_{79}N_2O_6P$	SM(d18:1/16:0)	1	I
MF1571	209.09218	$[M+H]^+$	$C_{10}H_{12}N_2O_3$	DL-kynurenine	1	II
MF977	204.12317	$[M+H]^+$	$C_9H_{17}NO_4$	acetylcarnitine	1	II / IV
MF3513	288.28946	$[M+H]^+$	$C_{17}H_{37}NO_2$	sphinganine C17 isomer	2	I
MF3680	316.32092	$[M+H]^+$	$C_{19}H_{41}NO_2$	d19:0 sphinganine	2	I
MF3705	468.30853	$[M+H]^+$	$C_{22}H_{46}NO_7P$	LysoPC(14:0)	2	I
MF3760	280.26334	$[M+H]^+$	$C_{18}H_{33}NO$	linoleamide	2	I
MF3785	520.33990	$[M+H]^+$	$C_{26}H_{50}NO_7P$	LysoPC(18:2)	2	I
MF3813	568.33972	$[M+H]^+$	$C_{30}H_{50}NO_7P$	LysoPC(22:6)	2	I
MF3874	482.36057	$[M+H]^+$	$C_{24}H_{52}NO_6P$	LysoPC(O-16:0)	2	I
MF3890	546.35547	$[M+H]^+$	$C_{28}H_{52}NO_7P$	LysoPC(20:3)	2	I
MF3896	480.34500	$[M+H]^+$	$C_{24}H_{50}NO_6P$	LysoPC(P-16:0)	2	I
MF3935	508.37635	$[M+H]^+$	$C_{26}H_{54}NO_6P$	LysoPC(P-18:0)	2	I
MF3942	228.23218	$[M+H]^+$	$C_{14}H_{29}NO$	myristamide	2	I
MF3948	572.37097	$[M+H]^+$	$C_{30}H_{54}NO_7P$	LysoPC(22:4)	2	I
MF3966	548.37110	$[M+H]^+$	$C_{28}H_{54}NO_7P$	LysoPC(20:2)	2	I
MF4019	550.38665	$[M+H]^+$	$C_{28}H_{56}NO_7P$	LysoPC(20:1)	2	I
MF4092	282.27902	$[M+H]^+$	$C_{18}H_{35}NO$	oleamide	2	I
MF4103	417.24002	$[M+H]^+$	$C_{21}H_{37}O_6P$	cPA(18:2)	2	I
MF4138	393.23975	$[M+H]^+$	$C_{19}H_{37}O_6P$	cPA(16:0)	2	I
MF4208	299.25800	$[M+H]^+$	$C_{18}H_{34}O_3$	oxo-octadecanoic acid	3	I
MF912	280.13882	$[M+H]^+$	$C_{11}H_{21}NO_7$	fructosylvaline	2	II
MF1110	305.09775	$[M+H]^+$	$C_{11}H_{16}N_2O_8$	*N*-acetylaspartylglutamate	2	II / IV
MF1325	221.09201	$[M+H]^+$	$C_{11}H_{12}N_2O_3$	5-hydroxytryptophan	2	II / IV
MF3600	304.28445	$[M+H]^+$	$C_{17}H_{37}NO_3$	isopropanolamine myristate	3	I
MF3773	429.29990	$[M+H]^+$	$C_{27}H_{40}O_4$	spirostane-3,6-dione	3	I
MF4000	237.22133	$[M\text{-}NH_3]^+$	$C_{16}H_{28}O$	fragment of palmitoleamide	3	I
MF4001	254.24773	$[M+H]^+$	$C_{16}H_{31}NO$	palmitoleamide	3	I
MF4158	592.46985	$[M+H]^+$	$C_{32}H_{66}NO_6P$	CerP(d14:0/18:0)	3	I
MF4184	701.55886	$[M+H]^+$	$C_{39}H_{77}N_2O_6P$	SM(d18:1/16:1)	3	I
MF4195	689.55860	$[M+H]^+$	$C_{38}H_{77}N_2O_6P$	SM(d18:1/15:0)	3	I
MF1260	276.14404	$[M+H]^+$	$C_{12}H_{21}NO_6$	glutarylcarnitine	3	II
MF1314	233.09191	$[M+H]^+$	$C_{12}H_{12}N_2O_3$	indole-3-acetylglycine	3	II
MF1690	207.08774	$[M+H]^+$	$C_9H_{10}N_4O_2$	hypoxanthine derivative	3	II
MF3276	254.13862	$[M+H]^+$	$C_{13}H_{19}NO_4$	L-DOPA n-butyl ester	3	II
MF617	253.02943	$[M+H]^+$	$C_{12}H_{10}Cl_2N_2$	3,3-dichlorobenzidine	3	II
MF749	147.07629	$[M+H]^+$	$C_5H_{10}N_2O_3$	DL-glutamine	3	II
MF905	168.02919	$[M+H]^+$	$C_7H_5NO_4$	quinolinic acid	3	II / IV
MF730	147.02869	$[M+H]^+$	$C_5H_6O_5$	oxoglutaric acid	3	IV
MF4021	548.37958	$[M+H]^+$	$C_{23}H_{50}N_9O_4P$	unclassified phospholipid	4	I
MF1088	312.11102	$[M+H]^+$	$C_{11}H_{21}NO_7S$	*N*-(1-deoxy-1-fructosyl)methionine	4	II
MF894	339.14096	$[M+H]^+$	$C_{13}H_{18}N_6O_5$	purine nucleoside	4	II
MF622	231.04753	$[M+H]^+$	$C_{13}H_{10}SO_2$	unidentified	4	III
MF742	437.97220	$[M+H]^+$	$C_{11}H_7N_3O_{14}S$	unidentified	4	III
MF895	248.06425	$[M+H]^+$	$C_7H_5N_9O_2$	unidentified	4	III
MF2294	594.61349	$[M+3H]^{3+}$	-	unidentified	5	III
MF400	271.96494	$[M+H]^+$	-	unidentified	5	IV

*MF identifications were assigned according to the five-level system, based on the Metabolomics Standards Initiative (MSI) framework, which defines minimum reporting standards for metabolomics studies (Schymanski et al., 2014; Sumner et al., 2007).

to tentative annotation based on MS/MS spectral matching with literature or databases. **Level 3** comprised 42 MFs, with tentative candidate structure supported by molecular formula and MS/MS spectral information. **Level 4** accounted for 27 MFs, corresponding to features assigned with matching molecular formula, isotopic pattern, possible adduct formation, and charge state. Finally, **Level 5** included 3 MFs, representing unclassified yet distinct mass spectral features. Comprehensive characterization of all 131 MFs, with their classification categories and MSI levels, are presented in **Supplementary Table S1**, while an example subset of 49 features is summarized in Table 2.

MSE analysis was performed using the MetaboAnalyst platform with RaMP-DB as the reference for pathway associations. The 25 most significant ($p < 0.05$) metabolomic and molecular pathways are shown in Fig. 5. The analysis highlighted several pathways of potential pathophysiological relevance in LNB and nine of the most significant metabolomic pathways clearly stood out.

4. Discussion

In this study, we performed untargeted UHPLC-MS/MS-based metabolite profiling of LNB patients and control CSF samples to investigate metabolic alterations associated with acute LNB. We compared the acute pretreatment LNB CSF samples to three weeks' time point samples after treatment initiation of the same individuals (comparison **A**), age- and sex-matched non-LNB control CSF samples (comparison **B**), and CSF samples of subjects with other laboratory confirmed CNS infections (TBE, HSV, and VZV) (comparison **C**). With these comparisons we aimed to characterize the metabolic features of LNB. Additionally, we explored LNB manifestation-associated variability in the CSF metabolite profiles by comparing acute pretreatment LNB subjects with and without radiculitis (comparison **D**). Out of 4222 detected MFs, 131 MFs were selected for detailed evaluation based on statistical significance, magnitude of change, and structural characterization. These MFs provide insights into both general infection-related and disease-specific metabolic responses in LNB, offering potential CSF biomarkers for the disease.

In comparison **A,** the metabolites prominent in the LNB pretreatment CSF samples were statistically significantly related to tryptophan metabolism and lipid signaling pathways, many of which were also associated with CSF CXCL13 concentration, a marker of LNB inflammation (Hytönen et al., 2014; Waiß et al., 2024). Most metabolites with increased concentration in the pretreatment LNB samples were decreasing at three weeks after treatment initiation (excluding MFs that were associated with antibiotic treatment).

Comparison **B** confirmed the specificity of several acute-phase alterations, distinguishing LNB from non-LNB individuals and supporting the pathological specificity of these metabolomic changes. In addition, shared metabolites between comparisons **A** and **B** suggest the possibility for identifying both disease-specific and general infection biomarkers in future studies.

Comparison **C** revealed a set of metabolic changes shared across infectious CNS diseases, as well as those more specific to LNB. However, only a few of the shared MFs fell outside **category V** or the exogenous MFs in **category II**; one example is acetylcarnitine, which can be considered also as a general biomarker of infection.

Comparison **D**, which compared acute LNB subjects by the presence

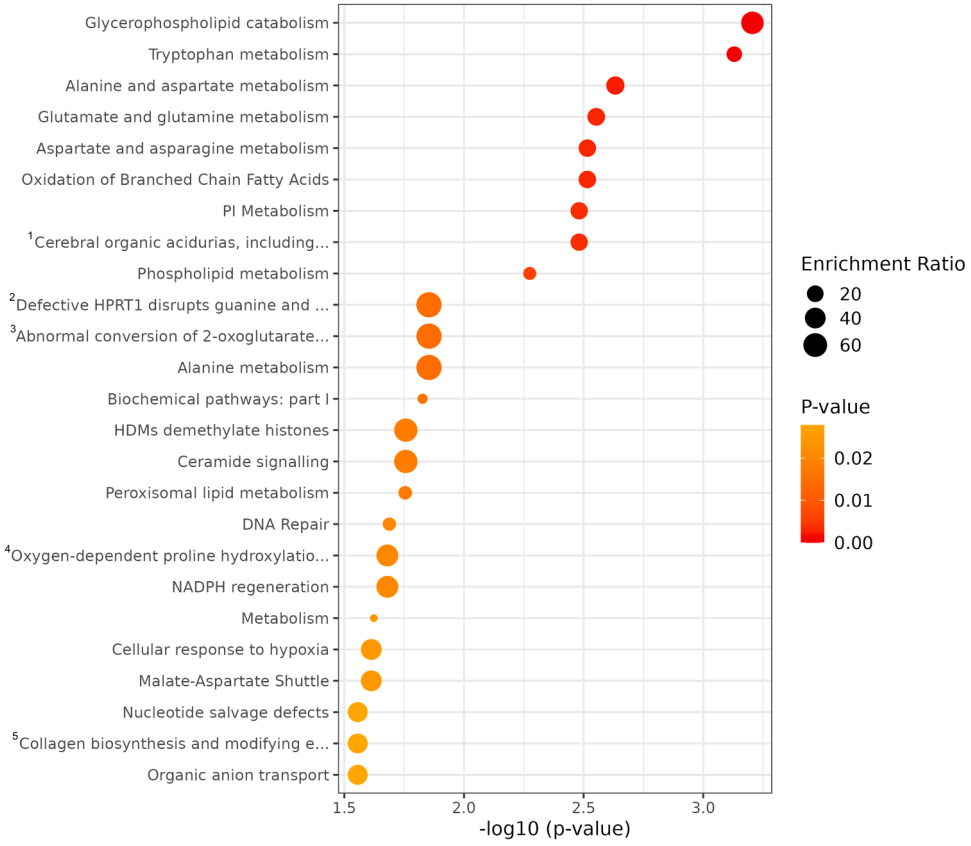

Fig. 5. Metabolite set enrichment (MSE) analysis dot plot of the 25 most significant metabolite/molecular pathways ($p < 0.05$). The y-axis lists pathways and the x-axis shows $-\log_{10}$ (p-value), so circles further to the right indicate greater statistical significance. Circle size encodes the enrichment ratio, and circle color encodes the nominal p-value (warmer/red tones indicate lower p-values, cooler/yellow tones higher p-values). Only pathways meeting the significance threshold are displayed. Pathways with truncated labels (1–5) on the y-axis are as follows: [1]Cerebral organic acidurias, including diseases; [2]Defective HPRT1 disrupts guanine and hypoxanthine salvage; [3]Abnormal conversion of 2-oxoglutarate to 2-hydroxyglutarate; [4]Oxygen-dependent proline hydroxylation of hypoxia-inducible factor alpha; [5]Collagen biosynthesis and modifying enzymes.

or absence of radiculitis prior to antibiotic treatment, revealed fewer significant metabolic differences under the applied analytical parameters. This finding may reflect the complex influence of radiculitis on the CSF metabolome or the challenges posed by subgroup heterogeneity within patient subgroups. Importantly, previous research has shown that LNB patients with meningoradiculoneuritis (Garin-Bujadoux-Bannwarth syndrome) exhibit a distinct immune profile compared to those without radiculoneuritis (Ogrinc et al., 2022), supporting the rationale for evaluating metabolite profiles along this clinical axis.

Across the CSF samples, a total of 76 MFs were classified as **category I** metabolites (lipids and lipid-type compounds). MFs in this category consist of lysophospholipids (LysoPLs), sphingolipids, primary fatty acid amides, cyclic phosphatidic acids (cPAs) and other lipid-related MFs (see Table 2 and **Supplementary Table S1)**.

LysoPLs are monoacyl derivatives of phospholipids, commonly present in CSF and are involved in membrane remodeling and intracellular signaling pathways (Choi and Chun, 2013; Wepy et al., 2019). In this study, the LysoPL category was subdivided into lysophosphatidylcholines (LysoPCs) and lysophosphatidylethanolamines (LysoPEs). Łuczaj et al. (2025) previously reported significant alterations in LysoPC levels in plasma from LNB patients, changes associated with phospholipase A_2 activity and membrane remodeling, suggesting heightened inflammatory responses during CNS infection. In the present study, we identified the same LysoPCs, MF3825 and MF3781 as isomers of [LysoPC(16:0)] (Jiang et al., 2023; Park et al., 2020), and MF3813 as [LysoPC(22:6)] (Wu et al., 2020b; Zhang et al., 2023a), confirming their relevance in LNB-related metabolic changes.

More broadly, disruptions in LysoPC species have been reported in neuroinflammatory conditions such as multiple sclerosis, implicating also phospholipase A_2 activity in membrane remodeling and inflammation (Stoessel et al., 2018). In the present study, we identified several of the same LysoPC MFs, including MF3896 [LysoPC(P-16:0] (Mohsenian Kouchaksaraee et al., 2020), MF3935 [LysoPC(P-18:0)] (Mohsenian Kouchaksaraee et al., 2020), MF3892 /MF3910 [LysoPC (18:1)] (Jiang et al., 2023), MF3933 [(2R)-2,8-dimethyl-2-(4,8, 12-trimethyltrideca-3,7,11-trienyl)-3,4-dihydrochromen-6-ol] (Beretta et al., 2018), LysoPC(20:0), MF4011 [LysoPC(O-18:0)] (Mohsenian Kouchaksaraee et al., 2020), MF4013 [LysoPE(P-18:0)] (Wu et al., 2020a), MF4019 [LysoPC(20:1)] (Fu et al., 2024) and MF3890 [LysoPC (20:3)] (Jiang et al., 2023). Furthermore, Ren et al. (2025) demonstrated that LysoPC(18:1) levels increase in serum, dorsal root ganglion and CSF after peripheral nerve injury. Similar elevation can also be seen in comparison **B** of the current CSF analysis.

While direct CSF studies in LNB are limited, our findings suggest that altered LysoPC profiles are involved in LNB. This supports further investigation of other characterized LysoPLs such as MF3705 [LysoPC (14:0)] (Jiang et al., 2023), MF3745 [LysoPC(16:1)] (Wu et al., 2020b), MF3757 [LysoPC(15:0)] (Jiang et al., 2023), MF3785 [LysoPC(18:2)] (Jiang et al., 2023), MF3799 [LysoPC(20:4)] (Jiang et al., 2023), MF3874 [LysoPC(O-16:0)] (Mohsenian Kouchaksaraee et al., 2020), MF3884 [LysoPC(22:5)] (Yan et al., 2025), MF3888 [LysoPE(16:0)] (Jiang et al., 2022), MF3928 / MF3906 [LysoPC(17:0)] (Ji et al., 2022; Li et al., 2014), MF3948 [LysoPC(22:4)] (Zhang et al., 2023b), MF3966 [LysoPC(20:2)] (Ji et al., 2022), MF3981 [LysoPE(18:0)] (Fang et al., 2003) and MF3987 [LysoPC(18:0)] (Park et al., 2020).

Five sphingoid bases (long-chain amino alcohols forming the structural backbone of sphingolipids) were significantly increased in the pretreatment CSF samples of LNB patients, when compared to samples collected three weeks after treatment initiation and to samples from non-LNB controls. These MFs included d19:0 sphinganine (Huang et al., 2018; Quehenberger et al., 2010) (MF3680), and 3-ketosphingosine (Zhang et al., 2024) (MF3921), suggesting perturbations in sphingolipid metabolism (Alaamery et al., 2021; Podbielska et al., 2022; Wang et al., 2024). These long-chain bases serve as precursors to complex sphingolipids in myelin and are recognized as bioactive signaling molecules. For example, in neuroinflammatory and demyelinating disorders such as multiple sclerosis, elevations of these sphingoid bases have been reported (Podbielska et al., 2022; Shi et al., 2025). However, sphingolipid MFs were not statistically highlighted in comparison **D**, but should be further investigated in the context of disseminated LB. Additionally, sphinganine C17 isomers (MF3513, MF3545, and MF3571) were also identified (Othman et al., 2012). These MFs are typically associated with synthetic sphingoid bases but have also been reported as metabolites produced by gut microbiota (Johnson et al., 2020; Stoffel et al., 1975).

Several sphingomyelin MFs, including MF4165 [SM(d18:1/14:0)] (Qu et al., 2018), MF4184 [SM(d18:1/16:1)] (Fonteh et al., 2015), MF4195 [SM(d18:1/15:0] (Jakobsson et al., 2025) and MF4215 [SM (d18:1/16:0)] (Fonteh et al., 2015) were detected in comparison **A** and comparison **B** (MF4165 and MF4184). These sphingomyelins are key constituents of myelin and cell membranes. In diseases such as Guillain–Barré syndrome and chronic inflammatory demyelinating polyradiculoneuropathy (CIDP), elevated CSF levels of sphingomyelin have been identified as reliable biomarkers of active demyelination and disease staging (Capodivento et al., 2021). Additionally, plasma from LNB subjects has shown increased levels of sphingolipid species [e.g., CerPCho(d18:1/24:1)], suggesting systemic sphingolipidosis during infection (Łuczaj et al., 2017). In comparison **A**, statistical analysis identified only one phosphoceramide sphingolipid MF4158 [CerP (d14:0/18:0)]. These findings highlight the potential utility of sphingomyelins as biomarkers of nervous system involvement in LNB. Notably, several sphingomyelin based MFs also showed a statistically significant association with CSF concentrations of CXCL13 in comparison **A**, further supporting their relevance to neuroinflammatory processes in LNB.

Multiple MFs, classified as fatty acid amides, were detected to be statistically significant, including linoleamide (André et al., 2021; Huang et al., 2025) (MF3760), myristamide (El-Kashak et al., 2025) (MF3942), palmitoleamide (Barupal and Fiehn, 2019; Lohani et al., 2024; Oka et al., 2024) (MF4001), and oleamide (Han et al., 2022; Oka et al., 2024) (MF4092), alongside their characteristic MS/MS fragment ions. Primary fatty acid amides are recognized as neurologically active lipids that modulate inflammation, neuronal signaling, and glial function (Castillo-Peinado et al., 2019; Divito and Cascio, 2013; Ezzili et al., 2010; Groth et al., 2023; Kim et al., 2019). Notably, oleamide, (amide of oleic acid), has been linked to anti-inflammatory effects in microglia via purinergic P2Y receptor activation (Kita et al., 2019), and is known to block intercellular gap-junction communication in glial cells (Guan et al., 1997). Additionally, oleamide accumulates in CSF in response to sleep deprivation and exhibits multireceptor interactions, including activity at gamma-aminobutyric acid, serotonin, and cannabinoid receptors (Akanmu et al., 2007; Fedorova et al., 2001). These findings emphasize oleamide's neuromodulatory and immunoregulatory roles.

Two cPAs, MF4138 [cPA(16:0)] (Shimizu et al., 2018; Tokumura et al., 1982) and MF4103 [cPA(18:2)] (Shimizu et al., 2018), were identified in comparison **A** and comparison **B** (MF4138). Structurally cPAs are distinct bioactive lipids that differ from lysophosphatidic acids by their cyclic phosphate rings at the sn-2 and sn-3 positions. They have been shown to inhibit cell proliferation, migration, and neuroinflammatory responses (Gotoh et al., 2012; Uchiyama et al., 2007). For example, both cPA(16:0) and cPA(18:1) have demonstrated neuroprotective effects in models of ischemic brain injury and hypoxia-induced neuronal death by modulating pathways linked to lysophosphatidic acid receptors (Gotoh et al., 2012). Notably, both cPA species were statistically associated with CXCL13 concentrations, indicating a possible link between cPA signaling and chemokine-mediated immune activation. These findings underscore the relevance of cPAs as endogenous modulators of neuroinflammation and support their further investigation as potential biomarkers for LNB.

Additional lipid-associated MFs, including spirostane-3,6-dione (Mesa et al., 2023) isomers (MF3773 and MF3883), valenciaxanthin (Märki-Fischer and Eugster, 1990) (MF4069), methyl-12-oxo-octadecanoate (Mizota et al., 2016) (MF4119) and

fragment ion of phosphorylcholine (Guerra et al., 2023) (MF4212) and oxo-octadecanoic acid (Márquez-Ruiz et al., 2011) (MF4208), were detected. The biological relevance of these compounds in the context of LNB is currently unclear and remains to be determined. Future studies are needed to elucidate their potential roles in CNS infection and in LNB.

Several endogenous and exogenous MFs (**category II**), were highlighted by statistical analysis, warranting further investigation. The presence of endogenous neuroactive intermediates including DL-kynurenine (MF1571) and 5-hydroxytryptophan (Di Matteo and Petrucci, 2025; Liang et al., 2023) (MF1325), acetylcarnitine (Chung et al., 2019; Cowan et al., 2016; Ferreira and McKenna, 2017; Nasca et al., 2018) (MF977), glutarylcarnitine (Mohamed et al., 2015; Sun et al., 2020) (MF1260), and DL-glutamine (Guo et al., 2021; Welbourne, 1979; Wilmore and Shabert, 1998) (MF749) suggest possible alterations to amino acid metabolism. Moreover, acetylcarnitine has demonstrated neuroprotective effects in brain injury models, improving mitochondrial bioenergetics and reducing oxidative stress (Ferreira and McKenna, 2017). Glycation-related metabolite *N*-(1-deoxy-1-fructosyl)methionine (Yang et al., 2023) (MF1088), may reflect elevated protein turnover or oxidative protein damage (Ahmed et al., 2005). Also, endogenous citryl-L-glutamic acid (Miyake et al., 1978) (MF1046) and purine nucleoside (Huang et al., 2025) (MF894) were detected. Lastly, exogenous or xenobiotic features i.e. possible 5-hydroxymethyl-3,4-piperidinediol (Barupal and Fiehn, 2019; Imahori et al., 2008; Rives et al., 2009) (MF613), 3,3-dichlorobenzidine (Barupal and Fiehn, 2019; Ning et al., 2015) (MF617), 5-hydroxy-2-furoic acid (Barupal and Fiehn, 2019) (MF735), fructosylvaline (Barupal and Fiehn, 2019) (MF912), indole-3-acetylglycine (Feung et al., 1975) (MF1314) and L-DOPA n-butyl ester (Barupal and Fiehn, 2019) (MF3276) likely originate from environmental sources.

A subset of eight detected MFs in our CSF metabolomic analysis remained unidentified (**category III**). These unknown compounds eluted across a broad RT area, indicating substantially different physicochemical properties. Their reproducible detection across multiple samples suggests potential biological relevance. However, the accurate identification of these metabolites is challenging, even when using exact mass measurements, MS/MS, and comprehensive spectral libraries and databases (Guo et al., 2022). Their categorization and annotation could benefit from increasingly advanced data processing techniques and predictive tools, such as molecular networking and artificial intelligence-based tools (Harris et al., 2022; Kuukkanen et al., 2026; Nothias et al., 2020; Petrick and Shomron, 2022).

Eight MFs (MF400, MF730, MF905, MF1110, MF1325, MF1363, MF1566 and MF1769) classified as **category IV** metabolites in comparisons **A** and **B**, were not identified as medicinal compounds. However, they showed noticeable statistical associations with APAP use, suggesting possible drug-induced metabolic effects. MF400 and MF1769 were unidentified, and their molecular formulae remain yet unknown. MF1769 was present in both comparisons **A** and **B**. These results show that medication should be considered as a potential confounding factor in biomarker identification.

Of the above mentioned MFs, MF730 was identified as oxoglutaric acid (Harrison and Pierzynowski, 2008; Hounguè et al., 2022; Wu et al., 2016), and MF905 as quinolinic acid (Zhao et al., 2020), a neuroactive metabolite within the kynurenine pathway of tryptophan metabolism. It is known as a biomarker of neuroinflammation and excitotoxicity due to its agonist activity at *N*-methyl-D-aspartate (NMDA) receptors, and elevated CSF concentrations of quinolinic acid have been observed in subjects with Bbsl-associated nervous system inflammation (Ahlberg Weidenfors et al., 2025; Guillemin, 2012; Halperin and Heyes, 1992; Obrenovitch, 2001; Schwarcz et al., 2012), correlating with elevated cytokines. This is the case also in comparison **A** where subject group together with CXCL13 cytokine concentration are statistically significant variables. In comparison **B,** subject group had the largest statistical weight, but also subject age and APAP use are statistically significant. Although quinolinic acid is not a product of APAP metabolism, APAP (and acetylsalicylic acid) has been shown in animal models to inhibit quinolinic acid-induced lipid peroxidation and oxidative neuronal damage (Maharaj et al., 2006). This suggests that APAP may have indirect neuroprotective effects against quinolinic acid accumulation in the brain. In our study, quinolinic acid was classified among MFs statistically associated with APAP use (**category IV**) and identified among endogenous metabolites in another (**category II**), underscoring its dual significance as both a medication-responsive and disease-related general biomarker.

MF1110 was characterized as dipeptide *N*-acetylaspartylglutamate (Sun et al., 2025; Xue et al., 2025), known to be one of the most abundant neuropeptides in the CNS (Guarda et al., 1988; Vallianatou et al., 2021), and shown to bond with metabotropic glutamate receptor 3 to modulate synaptic glutamate release and protect against excitotoxicity (Neale and Yamamoto, 2020). In the context of nervous system infections, such as LNB, excitotoxicity and neuroinflammation are common pathological features. Although *N*-acetylaspartylglutamate is not a direct metabolite of APAP, APAP has demonstrated neuroprotective properties against excitotoxic damage *in vitro* and in animal models, as mentioned before, likely by attenuating glutamate-mediated oxidative stress and inflammation (Maharaj et al., 2006; Tripathy and Grammas, 2009). Here, *N*-acetylaspartylglutamate was statistically linked with APAP use (comparison **B**), suggesting that APAP's neuroprotective effects may involve modulation of endogenous glutamate release. Subject group was also statistically significant variable of *N*-acetylaspartylglutamate. These findings suggests that *N*-acetylaspartylglutamate could function as a potential **category II** biomarker, providing an indication of neuroinflammatory status and possibly treatment response in nervous system infections complicated by medication use (**category IV**). However, its specificity and clinical utility require further investigation.

MF1363 was identified as a dehydration fragmentation product of 5-hydroxytryptophan, formed during the MS/MS analysis. 5-hydroxytryptophan serves as a precursor to serotonin and is known to cross the blood–brain barrier efficiently, facilitating central serotonergic regulation (Birdsall, 1998; Sharma et al., 2019). In our metabolomic analysis, both MFs were statistically linked with APAP use (comparison **B**), but strongly also to subject group and subject age. Serving as both an endogenous neurochemical marker (**category II**) and a medication-associated feature (**category IV**), highlights the importance of accounting for pharmacological influences when interpreting metabolomic signatures in nervous system infections.

Similarly, MF1566 and MF1563 were identified as fragmentation products of DL-kynurenine (Barré et al., 2019; Duarte et al., 2019) (MF1571, $C_{10}H_{12}N_2O_3$) during MS/MS analysis. MF1566 ($C_{10}H_9NO_3$) results from the loss of an amino group (–NH_3), while MF1563 (C_9H_7NO) is formed through cleavage of the NH_3–COOH moiety (MF1571, $C_{10}H_{12}N_2O_3$) during MS/MS analysis. The identification of DL-kynurenine was confirmed against a reference standard. Kynurenine itself did not show a statistically significant association with medication use, in contrast to its fragment ions. Nevertheless, activation of the tryptophan pathway is a well-established feature of CNS infections and has been implicated in the pathogenesis of neuroinflammation. Elevated levels of kynurenine and its downstream metabolites, including neuroactive compounds such as kynurenic acid and quinolinic acid, have been consistently reported in CSF from subjects with bacterial meningitis and other CNS infections. Coutinho et al. (2014) demonstrated significant increases in these metabolites in bacterial meningitis, underscoring the pathway's involvement in the inflammatory response within the CNS. Furthermore, in a study by Sühs et al. (2019) CSF levels of kynurenine and the kynurenine/tryptophan ratio effectively distinguished between non-infectious and infectious neurological conditions, including LNB, bacterial meningitis, and viral CNS infections. This may explain why kynurenine and its MS/MS fragmentation products emerged as statistically significant in comparisons **A** and **B**, but not in comparison **C**, which focused on other CNS infections (TBE, HSV and VZV). In comparison **A**,

both MF1563 and MF1571 showed no statistically significant association with APAP use (identified as **category II** MF), with the comparison itself being the primary explanatory factor. In comparison **B**, MF1566 was influenced by APAP use (identified as **category IV** MF); however, the subject group remained the most significant variable. These findings support the role of kynurenine pathway metabolites as biomarkers of CNS immune activation and highlight their potential diagnostic value in distinguishing LNB from other neurological conditions.

A total of 26 characterized MFs were identified as either directly derived from medications or strongly associated with their use. Specifically, 19 MFs were classified under **category V**, representing compounds originating from medication. Of these, 16 MFs were attributed to the analgesic APAP (MF1713) (Dargue et al., 2020; David et al., 2021) and its known phase I and phase II metabolic derivatives with other minor metabolites, including features reflecting typical mass shifts, fragment ions, or adduct ions (Dargue et al., 2020; David et al., 2021; Hairin et al., 2013; Rousar et al., 2023; Zhang et al., 2018). For more detailed characterization of these MFs see **Supplementary Table S1**. Five of the APAP-related MFs could not be precisely annotated, for example, due to the absence of high-confidence MS/MS spectral data. However, these unidentified APAP derived MFs (MF1456, MF1707, MF1708, MF1716, MF1717 and MF1721), displayed similar molecular formulae, MS/MS spectra (excluding MF1456, MF1707 and MF1716) and a strong statistically similar behavior to those of the well-characterized APAP derived MFs [MF1437, MF1441 (David et al., 2021), MF1442 (Dargue et al., 2020; Noda et al., 2022; Zhang et al., 2018), MF1518 (Dargue et al., 2020; David et al., 2021; Rousar et al., 2023), MF1658 (Dargue et al., 2020), MF2017 (David et al., 2021) and MF2484, supporting their classification as directly APAP-derived metabolites.

Doxycycline (Gajda et al., 2014; Sapon et al., 2017) and its related MFs (MF2235 and MF2978) were statistically significant in comparison **A**, with MS signals observed only in the pretreatment LNB subgroup receiving doxycycline at the three-week time point (Kortela et al., 2021). This observation supports the sensitivity and analytical accuracy of the applied method. In contrast, no MFs associated with ceftriaxone or its metabolites reached statistical significance. However, ceftriaxone was detected in patients receiving the medication (n = 14) in comparison **A**. Lower MS peak areas in the CSF samples of these patients compared with doxycycline (n = 22) can be explained by combined pharmacokinetic and analytical factors. Ceftriaxone is highly bound to protein, restricting the free fraction available for CNS penetration, as only unbound drug can cross the blood–brain barrier (Nau et al., 2010). Whereas doxycycline is more lipophilic and achieves more consistent CSF penetration, typically ~10–30% of serum concentrations (Haddad et al., 2022). From an analytical perspective, ceftriaxone's polarity and interaction with proteins and Ca^{2+} ions can reduce extraction efficiency and increase matrix effects in MS analysis, while doxycycline's lipophilicity favors recovery (Krishna et al., 2012; Sun et al., 2022; Wongchang et al., 2022). Additionally, ESI efficiency can differ between compounds (Kamel et al., 1999; Wongchang et al., 2022). Pharmacokinetically, ceftriaxone exhibits delayed and inflammation-dependent CSF entry with substantial interindividual variability (Buke, 2003; Haddad et al., 2022; Kumta et al., 2025), whereas doxycycline shows more stable exposure due to its longer half-life and more predictable penetration into CSF (Haddad et al., 2022).

MSE analysis identified many affected metabolic pathways. Alterations in glycerophospholipid catabolism and phosphatidylinositol metabolism are consistent with prior phospholipidomic studies demonstrating disturbances in lysophosphatidylcholine and sphingomyelin species in plasma of subjects with LNB (Łuczaj et al., 2017). Enrichment of amino acid–related pathways, including tryptophan, alanine and aspartate, glutamate and glutamine, and aspartate and asparagine metabolism, aligns with reports showing that tryptophan degradation via the kynurenine pathway is elevated in acute LNB and other tick-borne infections (Ahlberg Weidenfors et al., 2025; Coutinho et al., 2014; Gasse et al., 1994; Halperin and Heyes, 1992; Sühs et al., 2019). In addition, kynurenine pathways have been shown to be differentially activated in children with LNB and TBE (Wickström et al., 2021). Enrichment of branched-chain fatty acid oxidation suggests alterations in mitochondrial energy metabolism, in line with evidence that disruptions in fatty acid oxidation led to mitochondrial stress and acylcarnitine accumulation (Guerra et al., 2022), with similar metabolic changes also observed in early LB subject's serum (Fitzgerald et al., 2020). Finally, pathways linked to cerebral organic acidurias may reflect the accumulation of metabolic intermediates and overlap with neurotoxic mechanisms in inflamed CSF.

This study has certain limitations. As the samples were of clinical origin, they were not stored under the optimal −80 °C conditions, which may have affected the metabolomic profiles of the subjects. Detailed clinical information was unavailable for control samples from non-LNB and other CNS infection cases (e.g., pleocytosis status). Furthermore, the demonstrated complexity and richness of the CSF lipidome, particularly under inflammatory states, suggest that alternative sample pretreatment strategies and the use of UHPLC–MS/MS methods optimized for more hydrophobic metabolites could provide additional insights. It should also be noted that some lipid subclasses may have been underrepresented due to their late RTs. Also, some MFs remained unidentified despite using high-resolution MS/MS and spectral databases, emphasizing the current gaps in chemical annotation capabilities, especially for novel or trace level metabolites. These so far unknown compounds, which eluted across the entire chromatographic area, could serve as potential LNB biomarkers in future as well.

5. Conclusions

Our untargeted metabolomic analysis of CSF samples from subjects with LNB revealed a diverse array of metabolic alterations linked to neuroinflammation, immune activation, and CNS pathophysiology. Different metabolite classes, such as LysoPLs, SMs, sphingoid bases, fatty acid amides, and cPAs were significantly altered, suggesting roles in membrane remodeling, myelin turnover, and neuroimmune regulation. Pathways involving tryptophan catabolism (e.g., DL-kynurenine), neurotransmitter precursors (e.g., 5-hydroxytryptophan), and mitochondrial function (e.g., acetylcarnitine) were also implicated.

While the study revealed compelling associations between specific metabolites and clinical markers such as CSF CXCL13 concentration, its cross-sectional design limits our ability to draw conclusions about cause-and-effect relationships. Nevertheless, these findings offer a valuable foundation for future research. The study identifies several promising biomarker candidates and provides new insights for understanding the metabolic profile of LNB. Larger subject cohorts will be essential to confirm and validate the diagnostic and prognostic potential of these biomarkers. Importantly, our results suggest that CSF metabolomics could be useful complementary tool in the diagnosis of LNB.

Abbreviations

APAP	acetaminophen (paracetamol)
CNS	central nervous system
CSF	cerebrospinal fluid
CerP	phosphoceramide
cPA	cyclic phosphatidic acid
CXCL13	chemokine (C-X-C motif) ligand 13
EFNS	European Federation of Neurological Societies
HMDB	Human Metabolome Database
HSV	Herpes simplex virus
LB	Lyme borreliosis
LNB	Lyme neuroborreliosis
LysoPC	lysophosphatidylcholine
LysoPE	lysophosphatidylethanolamine
LysoPL	lysophospholipid
MF	molecular feature
MS	mass spectrometry
MSE	metabolite set enrichment

(*continued on next page*)

(*continued*)

MSI	The Metabolomics Standards Initiative
MS/MS	tandem mass spectrometry
non-LNB	*Borrelia burgdorferi* sensu lato antibody-negative control subject
RaMP-DB	Relational database of Metabolomic Pathways
SM	sphingomyelin
TBE	tick-borne encephalitis
UHPLC	ultrahigh-performance liquid chromatography
VZV	Varicella zoster virus

Funding and additional information

The research was funded by the University of Turku, a grant from the Turku University Foundation to IK (081451), two grants from Sakari Alhopuro Foundation to AP (20230181 and 20200177) and Academy project funding from Research Council of Finland (362569).

Declaration of AI-assisted technologies in the writing process

During the preparation of the manuscript, Microsoft Copilot was used to assist with rephrasing and improving grammar. All content generated with the help of this tool was subsequently reviewed, edited, and approved by the author(s), who take full responsibility for the final version of the publication. No AI assistance was used in the generation, analysis, or interpretation of scientific content.

Data availability

The UHPLC-MS/MS raw data and the processed data from Compound Discoverer™ analyses used in this study are available on request from the corresponding author.

Supporting information: This article contains supporting information.

CRediT authorship contribution statement

Ilari Kuukkanen: Writing – review & editing, Writing – original draft, Visualization, Validation, Software, Methodology, Investigation, Funding acquisition, Formal analysis, Data curation, Conceptualization. **Annukka Pietikäinen:** Writing – review & editing, Resources, Project administration, Funding acquisition, Data curation, Conceptualization. **Tiia Rissanen:** Writing – review & editing, Visualization, Software, Investigation, Formal analysis. **Saija Hurme:** Writing – review & editing, Supervision. **Elisa Kortela:** Writing – review & editing, Conceptualization. **Jukka Hytönen:** Writing – review & editing, Supervision, Resources, Project administration, Investigation, Funding acquisition, Conceptualization. **Maarit Karonen:** Writing – review & editing, Supervision, Resources, Methodology, Investigation, Funding acquisition, Conceptualization.

Declaration of competing interest

J.H. is a part time consultant for the diagnostic company Reagena (Toivala, Finland). Other authors declare that they have no conflicts of interest with the contents of this article.

Acknowledgements

The authors thank all members of the Natural Chemistry Research Group and the Tick-borne Diseases Turku (TBD Turku) consortium for their valuable assistance and scientific discussions.

Supplementary materials

Supplementary material associated with this article can be found, in the online version, at doi:10.1016/j.ttbdis.2026.102645.

Data availability

Data will be made available on request.

References

Ahlberg Weidenfors, J., Griška, V., Li, X., Pranckevičienė, A., Pakalnienė, J., Atlas, A., Franzén-Röhl, E., Piehl, F., Lindquist, L., Mickienė, A., Engberg, G., Schwieler, L., Erhardt, S., 2025. Dysregulation of the kynurenine pathway is related to persistent cognitive impairment in tick-borne encephalitis. Brain Behav. Immun. 125, 452–465. https://doi.org/10.1016/j.bbi.2025.02.005.

Ahmed, N., Ahmed, U., Thornalley, P.J., Hager, K., Fleischer, G., Münch, G., 2005. Protein glycation, oxidation and nitration adduct residues and free adducts of cerebrospinal fluid in Alzheimer's disease and link to cognitive impairment. J. Neurochem. 92, 255–263. https://doi.org/10.1111/j.1471-4159.2004.02864.x.

Akanmu, M., Adeosun, S., Ilesanmi, O., 2007. Neuropharmacological effects of oleamide in male and female mice. Behav. Brain Res. 182, 88–94. https://doi.org/10.1016/j.bbr.2007.05.006.

Alaamery, M., Albesher, N., Aljawini, N., Alsuwailm, M., Massadeh, S., Wheeler, M.A., Chao, C., Quintana, F.J., 2021. Role of sphingolipid metabolism in neurodegeneration. J. Neurochem. 158, 25–35. https://doi.org/10.1111/jnc.15044.

André, R., Guedes, R., López, J., Serralheiro, M.L., 2021. Untargeted metabolomic study of HepG2 cells under the effect of *Fucus vesiculosus* aqueous extract. Rapid Commun. Mass Spectrometry 35, e9197. https://doi.org/10.1002/rcm.9197.

Barré, F.P.Y., Paine, M.R.L., Flinders, B., Trevitt, A.J., Kelly, P.D., Ait-Belkacem, R., Garcia, J.P., Creemers, L.B., Stauber, J., Vreeken, R.J., Cillero-Pastor, B., Ellis, S.R., Heeren, R.M.A., 2019. Enhanced sensitivity using MALDI imaging coupled with laser postionization (MALDI-2) for pharmaceutical research. Anal. Chem. 91, 10840–10848. https://doi.org/10.1021/acs.analchem.9b02495.

Barupal, D.K., Fiehn, O., 2019. Generating the blood exposome database using a comprehensive text mining and database fusion approach. Environ. Health Perspect. 127, 097008. https://doi.org/10.1289/EHP4713.

Beretta, G., Gelmini, F., Fontana, F., Moretti, R.M., Montagnani Marelli, M., Limonta, P., 2018. Semi-preparative HPLC purification of δ-tocotrienol (δ-T3) from *Elaeis guineensis* Jacq. And *Bixa orellana* L. and evaluation of its in vitro anticancer activity in human A375 melanoma cells. Nat. Prod. Res. 32, 1130–1135. https://doi.org/10.1080/14786419.2017.1320793.

Birdsall, T.C., 1998. 5-Hydroxytryptophan: a clinically-effective serotonin precursor. Altern. Med. Rev. 3, 271–280.

Braisted, J., Patt, A., Tindall, C., Sheils, T., Neyra, J., Spencer, K., Eicher, T., Mathé, E.A., 2023. RaMP-DB 2.0: a renovated knowledgebase for deriving biological and chemical insight from metabolites, proteins, and genes. Bioinformatics 39, btac726. https://doi.org/10.1093/bioinformatics/btac726.

Branda, J.A., Steere, A.C., 2021. Laboratory diagnosis of Lyme borreliosis. Clin. Microbiol. Rev. 34, e00018–19. https://doi.org/10.1128/CMR.00018-19.

Buke, A., 2003. Does dexamethasone affect ceftriazone penetration into cerebrospinal fluid in adult bacterial meningitis. Int. J. Antimicrob. Agents 21, 452–456. https://doi.org/10.1016/S0924-8579(03)00041-4.

Capodivento, G., De Michelis, C., Carpo, M., Fancellu, R., Schirinzi, E., Severi, D., Visigalli, D., Franciotta, D., Manganelli, F., Siciliano, G., Beronio, A., Capello, E., Lanteri, P., Nobile-Orazio, E., Schenone, A., Benedetti, L., Nobbio, L., 2021. CSF sphingomyelin: a new biomarker of demyelination in the diagnosis and management of CIDP and GBS. J. Neurol. Neurosurg. Psychiatry 92, 303–310. https://doi.org/10.1136/jnnp-2020-324445.

Castillo-Peinado, L.S., López-Bascón, M.A., Mena-Bravo, A., Luque de Castro, M.D., Priego-Capote, F., 2019. Determination of primary fatty acid amides in different biological fluids by LC–MS/MS in MRM mode with synthetic deuterated standards: influence of biofluid matrix on sample preparation. Talanta 193, 29–36. https://doi.org/10.1016/j.talanta.2018.09.088.

Choi, J.W., Chun, J., 2013. Lysophospholipids and their receptors in the central nervous system. Biochimica et Biophysica Acta (BBA) - Mol. Cell Biol. Lipids 1831, 20–32. https://doi.org/10.1016/j.bbalip.2012.07.015.

Chung, K.-P., Chen, G.-Y., Chuang, T.-Y., Huang, Y.-T., Chang, H.-T., Chen, Y.-F., Liu, W.-L., Chen, Y.-J., Hsu, C.-L., Huang, M.-T., Kuo, C.-H., Yu, C.-J., 2019. increased plasma acetylcarnitine in sepsis is associated with multiple organ dysfunction and mortality: a multicenter cohort study. Crit. Care Med. 47, 210–218. https://doi.org/10.1097/CCM.0000000000003517.

Coutinho, L.G., Christen, S., Bellac, C.L., Fontes, F.L., de Souza, F.R.S., Grandgirard, D., Leib, S.L., Agnez-Lima, L.F., 2014. The kynurenine pathway is involved in bacterial meningitis. J. Neuroinflamm. 11, 169. https://doi.org/10.1186/s12974-014-0169-4.

Cowan, E., Kumar, P., Burch, K.J., Grieve, D.J., Green, B.D., Graham, S.F., 2016. Treatment of lean and diet-induced obesity (DIO) mice with a novel stable obestatin analogue alters plasma metabolite levels as detected by untargeted LC–MS metabolomics. Metabolomics 12, 124. https://doi.org/10.1007/s11306-016-1063-0.

Dargue, R., Grant, I., Nye, L.C., Nicholls, A., Dare, T., Stahl, S.H., Plumb, R.S., Lee, K., Jalan, R., Coen, M., Wilson, I.D., 2020. The analysis of acetaminophen (paracetamol) and seven metabolites in rat, pig and human plasma by U(H)PLC–MS. Bioanalysis 12, 485–500. https://doi.org/10.4155/bio-2020-0015.

David, A., Chaker, J., Léger, T., Al-Salhi, R., Dalgaard, M.D., Styrishave, B., Bury, D., Koch, H.M., Jégou, B., Kristensen, D.M., 2021. Acetaminophen metabolism revisited using non-targeted analyses: implications for human biomonitoring. Environ. Int. 149, 106388. https://doi.org/10.1016/j.envint.2021.106388.

Di Matteo, P., Petrucci, R., 2025. A novel selective and sensitive HPLC-ESI-tandem MS/MS method for indole structure-retaining metabolites of tryptophan: application in beverages. Beverages 11, 37. https://doi.org/10.3390/beverages11020037.
Divito, E.B., Cascio, M., 2013. Metabolism, physiology, and analyses of primary fatty acid amides. Chem. Rev. 113, 7343–7353. https://doi.org/10.1021/cr300363b.
Duarte, D., Amaro, F., Silva, I., Silva, D., Fresco, P., Oliveira, J.C., Reguengo, H., Gonçalves, J., Vale, N., 2019. Carbidopa alters tryptophan metabolism in breast cancer and melanoma cells leading to the formation of indole-3-acetonitrile, a pro-proliferative metabolite. Biomolecules 9, 409. https://doi.org/10.3390/biom9090409.
El-Kashak, W.A., Essa, A.F., Abdelhameed, M.F., Ahmed, Y.H., Abd Elkarim, A.S., Elghonemy, M.M., Ibrahim, B.M.M., Gaara, A.H., Mohamed, T.K., Elshamy, A.I., 2025. Unveiling the neuroprotective potential of *Ipomoea carnea* ethanol extract via the modulation of tau and β-secretase pathways in AlCl3-induced memory impairment in rats in relation to its phytochemical profiling. Inflammopharmacology 33, 2043–2068. https://doi.org/10.1007/s10787-025-01687-0.
Ezzili, C., Otrubova, K., Boger, D.L., 2010. Fatty acid amide signaling molecules. Bioorg. Med. Chem. Lett. 20, 5959–5968. https://doi.org/10.1016/j.bmcl.2010.08.048.
Fang, N., Yu, S., Badger, T.M., 2003. LC-MS/MS analysis of lysophospholipids associated with soy protein isolate. J. Agric. Food Chem. 51, 6676–6682. https://doi.org/10.1021/jf034793v.
Fedorova, I., Hashimoto, A., Fecik, R.A., Hedrick, M.P., Hanuš, L.O., Boger, D.L., Rice, K. C., Basile, A.S., 2001. Behavioral evidence for the interaction of oleamide with multiple neurotransmitter systems. J. Pharmacol. Exp. Ther. 299, 332–342. https://doi.org/10.1016/S0022-3565(24)29334-4.
Ferreira, G.C., McKenna, M.C., 2017. L-carnitine and acetyl-L-carnitine roles and neuroprotection in developing brain. Neurochem. Res. 42, 1661–1675. https://doi.org/10.1007/s11064-017-2288-7.
Feung, C.-Shieung., Hamilton, R.H., Mumma, R.O., 1975. Indole-3-acetic acid. Mass spectra and chromatographic properties of amino acid conjugates. J. Agric. Food Chem. 23, 1120–1124. https://doi.org/10.1021/jf60202a008.
Fitzgerald, B.L., Molins, C.R., Islam, M.N., Graham, B., Hove, P.R., Wormser, G.P., Hu, L., Ashton, L.V., Belisle, J.T., 2020. Host metabolic response in early Lyme disease. J. Proteome Res. 19, 610–623. https://doi.org/10.1021/acs.jproteome.9b00470.
Cyster, J.G., Ansel, K.M., Reif, K., Ekland, E.H., Hyman, P.L., Tang, H.L., Luther, S.A., Ngo, V.N., 2000. Follicular stromal cells and lymphocyte homing to follicles. Immunol. Rev. 176, 181–193. https://doi.org/10.1034/j.1600-065X.2000.00618.x.
Fonteh, A.N., Ormseth, C., Chiang, J., Cipolla, M., Arakaki, X., Harrington, M.G., 2015. Sphingolipid metabolism correlates with cerebrospinal fluid beta amyloid levels in Alzheimer's disease. PLoS One 10, e0125597. https://doi.org/10.1371/journal.pone.0125597.
Fu, J., Liang, Y., Yu, D., Wang, Y., Lu, F., Liu, S., 2024. Radix saposhnikoviae enhancing huangqi chifeng decoction improves lipid metabolism in as mice. J. Ethnopharmacol. 320, 117479. https://doi.org/10.1016/j.jep.2023.117479.
Gajda, A., Posyniak, A., Tomczyk, G., 2014. LC-MS/MS analysis of doxycycline residues in chicken tissues after oral administration. Bull. Veter. Inst. Pulawy 58, 573–579. https://doi.org/10.2478/bvip-2014-0089.
Gasse, T., Murr, C., Meyersbach, P., Schmutzhard, E., Wachter, H., Fuchs, D., 1994. Neopterin production and tryptophan degradation in acute Lyme neuroborreliosis versus late Lyme encephalopathy. CCLM 32, 685–690. https://doi.org/10.1515/cclm.1994.32.9.685.
Gotoh, M., Sano-Maeda, K., Murofushi, H., Murakami-Murofushi, K., 2012. Protection of neuroblastoma neuro2A cells from hypoxia-induced apoptosis by cyclic phosphatidic acid (cPA). PLoS One 7, e51093. https://doi.org/10.1371/journal.pone.0051093.
Grąźlewska, W., Holec-Gąsior, L., 2023. Antibody cross-reactivity in serodiagnosis of Lyme disease. Antibodies (Basel) 12, 63. https://doi.org/10.3390/antib12040063.
Groth, M., Skrzydlewska, E., Czupryna, P., Biernacki, M., Moniuszko-Malinowska, A., 2023. Lipid mediators of cerebrospinal fluid in response to TBE and bacterial co-infections. Free Radic. Biol. Med. 207, 272–278. https://doi.org/10.1016/j.freeradbiomed.2023.07.027.
Guan, X., Cravatt, B.F., Ehring, G.R., Hall, J.E., Boger, D.L., Lerner, R.A., Gilula, N.B., 1997. The sleep-inducing lipid oleamide deconvolutes gap junction communication and calcium wave transmission in glial cells. J. Cell Biol. 139, 1785–1792. https://doi.org/10.1083/jcb.139.7.1785.
Guarda, A.S., Robinson, M.B., Ory-Lavollée, L., Forloni, G.L., Blakely, R.D., Coyle, J.T., 1988. Quantitation of *N*-acetyl-aspartyl-glutamate in microdissected rat brain nuclei and peripheral tissues: findings with a novel liquid phase radioimmunoassay. Mol. Brain Res. 3, 223–231. https://doi.org/10.1016/0169-328X(88)90045-9.
Guerra, G., Segrado, F., Pasanisi, P., Bruno, E., Lopez, S., Raspagliesi, F., Bianchi, M., Venturelli, E., 2023. Circulating choline and phosphocholine measurement by a hydrophilic interaction liquid chromatography–tandem mass spectrometry. Heliyon 9, e21921. https://doi.org/10.1016/j.heliyon.2023.e21921.
Guerra, I.M.S., Ferreira, H.B., Melo, T., Rocha, H., Moreira, S., Diogo, L., Domingues, M. R., Moreira, A.S.P., 2022. Mitochondrial fatty acid β-oxidation disorders: from disease to lipidomic studies—A critical review. Int. J. Mol. Sci. 23, 13933. https://doi.org/10.3390/ijms232213933.
Guillemin, G.J., 2012. Quinolinic acid, the inescapable neurotoxin. FEBS J. 279, 1356–1365. https://doi.org/10.1111/j.1742-4658.2012.08485.x.
Gunn, M.D., Ngo, V.N., Ansel, K.M., Ekland, E.H., Cyster, J.G., Williams, L.T., 1998. A B-cell-homing chemokine made in lymphoid follicles activates Burkitt's lymphoma receptor-1. Nature 391, 799–803. https://doi.org/10.1038/35876.
Guo, H., Chen, Y.-H., Wang, T.-M., Kang, T.-G., Sun, H.-Y., Pei, W.-H., Song, H.-P., Zhang, H., 2021. A strategy to discover selective α-glucosidase/acetylcholinesterase inhibitors from five function-similar citrus herbs through LC-Q-TOF-MS, bioassay and virtual screening. J. Chromatogr. B 1174, 122722. https://doi.org/10.1016/j.jchromb.2021.122722.
Guo, J., Yu, H., Xing, S., Huan, T., 2022. Addressing big data challenges in mass spectrometry-based metabolomics. Chem. Commun. 58, 9979–9990. https://doi.org/10.1039/D2CC03598G.
Haddad, N., Carr, M., Balian, S., Lannin, J., Kim, Y., Toth, C., Jarvis, J., 2022. The blood–brain barrier and pharmacokinetic/pharmacodynamic optimization of antibiotics for the treatment of central nervous system infections in adults. Antibiotics 11, 1843. https://doi.org/10.3390/antibiotics11121843.
Hairin, T., Marzilawati, A.R., Didi, E.M.H., Mahadeva, S., Lee, Y.K., Abd. Rahman, N., Mustafa, A.M., Chik, Z., 2013. Quantitative LC/MS/MS analysis of acetaminophen–cysteine adducts (APAP–CYS) and its application in acetaminophen overdose patients. Analyt. Methods 5, 1955–1964. https://doi.org/10.1039/c3ay26614a.
Halperin, J.J., Heyes, M.P., 1992. Neuroactive kynurenines in Lyme borreliasis. Neurology 42, 43–50. https://doi.org/10.1212/WNL.42.1.43.
Hammers-Berggren, S., Hansen, K., Lebech, A.M., Karlsson, M., 1993. *Borrelia burgdorferi* -specific intrathecal antibody production in neuroborreliosis. Neurology 43, 169–175. https://doi.org/10.1212/WNL.43.1_Part_1.169.
Han, S., Kim, H., Lee, M.Y., Lee, J., Ahn, K.S., Ha, I.J., Lee, S.-G., 2022. Anti-cancer effects of a new herbal medicine PSY by inhibiting the STAT3 signaling pathway in colorectal cancer cells and its phytochemical analysis. Int. J. Mol. Sci. 23, 14826. https://doi.org/10.3390/ijms232314826.
Harris, M.B., Lesani, M., Liu, Z., McCall, L.-I., 2022. Molecular networking in infectious disease models. Meth. Enzymol. 663, 341–375. https://doi.org/10.1016/bs.mie.2021.09.018.
Harrison, A.P., Pierzynowski, S.G., 2008. Biological effects of 2-oxoglutarate with particular emphasis on the regulation of protein, mineral and lipid absorption/metabolism, muscle performance, kidney function, bone formation and cancerogenesis, all viewed from a healthy ageing perspective state of the art–review article. J. Physiol. Pharmacol. 59, 91–106. PMID: 18802218.
Hounguè, U., Villette, C., Tokoudagba, J.-M., Chaker, A.B., Remila, L., Auger, C., Heintz, D., Gbaguidi, F.A., Schini-Kerth, V.B., 2022. Carissa edulis Vahl (*Apocynaceae*) extract, a medicinal plant of Benin pharmacopoeia, induces potent endothelium-dependent relaxation of coronary artery rings involving nitric oxide. Phytomedicine 105, 154370. https://doi.org/10.1016/j.phymed.2022.154370.
Huang, D., Lv, J., Gong, W., Tian, J., Gao, X., Qin, X., Du, G., Zhou, Y., 2025. Combining metabolomics and quantitative analysis to investigate purine metabolism disorders in depression and the therapeutic effect of chaigui granules. ACS Chem. Neurosci. 16, 1749–1766. https://doi.org/10.1021/acschemneuro.4c00804.
Huang, H., Tong, T.-T., Yau, L.-F., Chen, C.-Y., Mi, J.-N., Wang, J.-R., Jiang, Z.-H., 2018. LC-MS based sphingolipidomic study on A549 human lung adenocarcinoma cell line and its taxol-resistant strain. BMC Cancer 18, 799. https://doi.org/10.1186/s12885-018-4714-x.
Hytönen, J., Kortela, E., Waris, M., Puustinen, J., Salo, J., Oksi, J., 2014. CXCL13 and neopterin concentrations in cerebrospinal fluid of patients with Lyme neuroborreliosis and other diseases that cause neuroinflammation. J. Neuroinflamm. 11, 103. https://doi.org/10.1186/1742-2094-11-103.
Imahori, T., Ojima, H., Yoshimura, Y., Takahata, H., 2008. Acceleration effect of an allylic hydroxy group on ring-closing enyne metathesis of terminal alkynes: scope, application, and mechanistic insights. Chem. – A Euro. J. 14, 10762–10771. https://doi.org/10.1002/chem.200801439.
Jakobsson, J.E., Menezes, J., Krock, E., Hunt, M.A., Carlsson, H., Vaivade, A., Emami Khoonsari, P., Agalave, N.M., Sandström, A., Kadetoff, D., Tour Sohlin, J., Erngren, I., Al-Grety, A., Freyhult, E., Sandor, K., Kosek, E., Svensson, C.I., Kultima, K., 2025. Fibromyalgia patients have altered lipid concentrations associated with disease symptom severity and anti-satellite glial cell IgG antibodies. J. Pain 29, 105331. https://doi.org/10.1016/j.jpain.2025.105331.
Jassal, B., Matthews, L., Viteri, G., Gong, C., Lorente, P., Fabregat, A., Sidiropoulos, K., Cook, J., Gillespie, M., Haw, R., Loney, F., May, B., Milacic, M., Rothfels, K., Sevilla, C., Shamovsky, V., Shorser, S., Varusai, T., Weiser, J., Wu, G., Stein, L., Hermjakob, H., D'Eustachio, P., 2019. The Reactome pathway knowledgebase. Nucleic Acids Res. 48, D498–D503. https://doi.org/10.1093/nar/gkz1031.
Ji, X., Chen, X., Sheng, L., Deng, D., Wang, Q., Meng, Y., Qiu, Z., Zhang, B., Zheng, G., Hu, J., 2022. Metabolomics profiling of AKT/c-Met-induced hepatocellular carcinogenesis and the inhibitory effect of cucurbitacin B in mice. Front. Pharmacol. 13, 1009769. https://doi.org/10.3389/fphar.2022.1009767.
Jiang, L., Yu, H., Wang, C., He, F., Shi, Z., Tu, H., Ning, N., Duan, S., Zhao, Y., 2022. The anti-cancer effects of mitochondrial-targeted triphenylphosphonium–resveratrol conjugate on breast cancer cells. Pharmaceuticals 15, 1271. https://doi.org/10.3390/ph15101271.
Jiang, S., Wei, X., Zhang, Y., Wang, Linna, Wang, Lianmei, Wang, M., Rong, Y., Zhou, J., Zhou, Y., Wang, H., Li, T., Si, N., Bian, B., Zhao, H., 2023. Biotransformed bear bile powder ameliorates diet-induced nonalcoholic steatohepatitis in mice through modulating arginine biosynthesis via FXR/PXR-PI3K-AKT-NOS3 axis. Biomed. Pharmacother. 168, 115640. https://doi.org/10.1016/j.biopha.2023.115640.
Johnson, E.L., Heaver, S.L., Waters, J.L., Kim, B.I., Bretin, A., Goodman, A.L., Gewirtz, A. T., Worgall, T.S., Ley, R.E., 2020. Sphingolipids produced by gut bacteria enter host metabolic pathways impacting ceramide levels. Nat. Commun. 11, 2471. https://doi.org/10.1038/s41467-020-16274-w.
Kalish, R.A., McHugh, G., Granquist, J., Shea, B., Ruthazer, R., Steere, A.C., 2001. Persistence of immunoglobulin M or immunoglobulin G antibody responses to *Borrelia burgdorferi* 10–20 years after active Lyme disease. Clin. Infect. Dis. 33, 780–785. https://doi.org/10.1086/322669.
Kamel, A.M., Brown, P.R., Munson, B., 1999. electrospray ionization mass spectrometry of tetracycline, oxytetracycline, chlorotetracycline, minocycline, and methacycline. Anal. Chem. 71, 968–977. https://doi.org/10.1021/ac9807114.

Kanehisa, M., Furumichi, M., Sato, Y., Matsuura, Y., Ishiguro-Watanabe, M., 2025. KEGG: biological systems database as a model of the real world. Nucleic Acids Res. 53, D672–D677. https://doi.org/10.1093/nar/gkae909.

Kim, M., Snowden, S., Suvitaival, T., Ali, A., Merkler, D.J., Ahmad, T., Westwood, S., Baird, A., Proitsi, P., Nevado-Holgado, A., Hye, A., Bos, I., Vos, S., Vandenberghe, R., Teunissen, C., ten Kate, M., Scheltens, P., Gabel, S., Meersmans, K., Blin, O., Richardson, J., De Roeck, E., Sleegers, K., Bordet, R., Rami, L., Kettunen, P., Tsolaki, M., Verhey, F., Sala, I., Lléo, A., Peyratout, G., Tainta, M., Johannsen, P., Freund-Levi, Y., Frölich, L., Dobricic, V., Engelborghs, S., Frisoni, G.B., Molinuevo, J. L., Wallin, A., Popp, J., Martinez-Lage, P., Bertram, L., Barkhof, F., Ashton, N., Blennow, K., Zetterberg, H., Streffer, J., Visser, P.J., Lovestone, S., Legido-Quigley, C., 2019. Primary fatty amides in plasma associated with brain amyloid burden, hippocampal volume, and memory in the European Medical Information Framework for Alzheimer's Disease biomarker discovery cohort. Alzheimer's & Dementia 15, 817–827. https://doi.org/10.1016/j.jalz.2019.03.004.

Kita, M., Ano, Y., Inoue, A., Aoki, J., 2019. Identification of P2Y receptors involved in oleamide-suppressing inflammatory responses in murine microglia and human dendritic cells. Sci. Rep. 9, 3135. https://doi.org/10.1038/s41598-019-40008-8.

Koedel, U., Fingerle, V., Pfister, H.-W., 2015. Lyme neuroborreliosis—Epidemiology, diagnosis and management. Nat. Rev. Neurol. 11, 446–456. https://doi.org/10.1038/nrneurol.2015.121.

Kortela, E., Kanerva, M.J., Puustinen, J., Hurme, S., Airas, L., Lauhio, A., Hohenthal, U., Jalava-Karvinen, P., Nieminen, T., Finnilä, T., Häggblom, T., Pietikäinen, A., Koivisto, M., Vilhonen, J., Marttila-Vaara, M., Hytönen, J., Oksi, J., 2021. Oral doxycycline compared to intravenous ceftriaxone in the treatment of Lyme neuroborreliosis: a multicenter, equivalence, randomized, open-label trial. Clin. Infect. Dis. 72, 1323–1331. https://doi.org/10.1093/cid/ciaa217.

Krishna, Ac., Sathiyaraj, M., Saravanan, R., Chelladurai, R., Vignesh, R., 2012. A novel and rapid method to determine doxycycline in human plasma by liquid chromatography tandem mass spectrometry. Indian J. Pharm. Sci. 74, 541. https://doi.org/10.4103/0250-474X.110599.

Kullberg, B.J., Vrijmoeth, H.D., van de Schoor, F., Hovius, J.W., 2020. Lyme borreliosis: diagnosis and management. BMJ 396, m1041. https://doi.org/10.1136/bmj.m1041.

Kumta, N., Heffernan, A.J., Liu, X., Parker, S.L., Cotta, M.O., Wallis, S.C., Livermore, A., Starr, T., Wai, W.T., Joynt, G.M., Lipman, J., Roberts, J.A., 2025. Ceftriaxone population pharmacokinetics in plasma and cerebrospinal fluid of neurocritical care patients. Int. J. Antimicrob. Agents 65, 107461. https://doi.org/10.1016/j.ijantimicag.2025.107461.

Kuukkanen, I., Muluh, G., Klisura, Đ., Kortela, E., Pietikäinen, A., Lahti, L., Hytönen, J., Karonen, M., 2026. Application of mass spectrometry-based metabolomics and machine learning in the diagnostics of Lyme neuroborreliosis. ACS Omega 11, 17521–17529. https://doi.org/10.1021/acsomega.5c10792.

Kuukkanen, I., Pietikäinen, A., Rissanen, T., Hurme, S., Kortela, E., Kanerva, M.J., Oksi, J., Hytönen, J., Karonen, M., 2025. UHPLC-MS/MS-based untargeted metabolite profiling of Lyme neuroborreliosis. Sci. Rep. 15, 8442. https://doi.org/10.1038/s41598-025-92189-0.

Li, Y., Zhang, X., Zhou, H., Fan, S., Wang, Y., Zhang, L., Ju, L., Wu, X., Wu, H., Zhang, Y., 2014. Metabonomics study on nephrotoxicity induced by intraperitoneal and intravenous cisplatin administration using rapid resolution liquid chromatography coupled with quadrupole-time-of-flight mass spectrometry (RRLC-Q-TOF-MS). RSC Adv 4, 8260–8270. https://doi.org/10.1039/C3RA46920D.

Liang, S.-S., Shen, P.-T., Liang, Y.-Q., Ke, Y.-W., Cheng, C.-W., Lin, Y.-R., 2023. Assisted reductive amination for quantitation of tryptophan, 5-hydroxytryptophan, and serotonin by ultraperformance liquid chromatography coupled with tandem mass spectrometry. Molecules 28, 4580. https://doi.org/10.3390/molecules28124580.

Lohani, H., Kumar, A., Bidarakundi, V., Agrawal, L., Haider, S.Z., Chauhan, N.K., 2024. Identification of fatty acids, amides and cinnamic acid derivatives in supercritical-CO_2 extracts of *Cinnamomum tamala* leaves using UPLC-Q-TOF-MSE combined with chemometrics. Molecules 29, 3760. https://doi.org/10.3390/molecules29163760.

Lu, Y., Pang, Z., Xia, J., 2023. Comprehensive investigation of pathway enrichment methods for functional interpretation of LC–MS global metabolomics data. Brief. Bioinform. 24, bbac553. https://doi.org/10.1093/bib/bbac553.

Łuczaj, W., Domingues, P., Domingues, M.R., Pancewicz, S., Skrzydlewska, E., 2017. Phospholipidomic analysis reveals changes in sphingomyelin and lysophosphatidylcholine profiles in plasma from patients with neuroborreliosis. Lipids 52, 93–98. https://doi.org/10.1007/s11745-016-4212-3.

Łuczaj, W., Moniuszko-Malinowska, A., Groth, M., Skrzydlewska, E., 2025. Changes in the serum phospholipid profile of neuroborreliosis patients, foresters, and patients subjected to long-term therapy according to ILADS methods. Prostaglandins Other Lipid Mediat 177, 106966. https://doi.org/10.1016/j.prostaglandins.2025.106966.

Maharaj, H., Maharaj, D.S., Daya, S., 2006. Acetylsalicylic acid and acetaminophen protect against oxidative neurotoxicity. Metab. Brain Dis. 21, 180–190. https://doi.org/10.1007/s11011-006-9012-7.

Märki-Fischer, E., Eugster, C.H., 1990. Struktur der Valenciaxanthine und Valenciachrome. Helv. Chim. Acta 73, 468–475. https://doi.org/10.1002/hlca.19900730227.

Márquez-Ruiz, G., Rodríguez-Pino, V., de la Fuente, M.A., 2011. Determination of 10-hydroxystearic, 10-ketostearic, 8-hydroxypalmitic, and 8-ketopalmitic acids in milk fat by solid-phase extraction plus gas chromatography-mass spectrometry. J. Dairy Sci. 94, 4810–4819. https://doi.org/10.3168/jds.2011-4424.

Mesa, D., Augusto, Y.E., Hernández, G., Figueroa-Macías, J.P., Coll, F., Olea, A.F., Núñez, M., Campo, H.A., Coll, Y., Espinoza, L., 2023. The synthesis of novel aza-steroids and α, β-unsaturated-cyanoketone from diosgenin. Molecules 28, 7283. https://doi.org/10.3390/molecules28217283.

Miyake, M., Kakimoto, Y., Sorimachi, M., 1978. Isolation and identification of β-citryl-L-glutamic acid from newborn rat brain. Biochimica et Biophysica Acta (BBA) - General Subjects 544, 656–666. https://doi.org/10.1016/0304-4165(78)90340-9.

Mizota, I., Umeshima, S., Matsunaga, S., Isomura, R., Nakahama, K., Shimizu, M., Yokomori, Y., Umemura, T., Kuroki, N., Kiyosawa, J., Tanaka, H., 2016. Exploration into a new dicarboxylic acid derived from ricinoleic acid for high-performance aluminum electrolytic capacitors. Bull. Chem. Soc. Jpn. 89, 1368–1374. https://doi.org/10.1246/bcsj.20160267.

Mohamed, S., Hamad, M.H., Hassan, H.H., Salih, M.A., 2015. Glutaric aciduria type 1 as a cause of dystonic cerebral palsy. Saudi Med. J. 36, 1354–1357. https://doi.org/10.15537/smj.2015.11.12132.

Mohsenian Kouchaksaraee, R., Moridi Farimani, M., Li, F., Nazemi, M., Tasdemir, D., 2020. Integrating molecular networking and 1H NMR spectroscopy for isolation of bioactive metabolites from the Persian Gulf sponge *Axinella sinoxea*. Mar. Drugs 18, 366. https://doi.org/10.3390/md18070366.

Mygland, Å., Ljøstad, U., Fingerle, V., Rupprecht, T., Schmutzhard, E., Steiner, I., 2010. EFNS guidelines on the diagnosis and management of European Lyme neuroborreliosis. Eur. J. Neurol. 17, 8–e4. https://doi.org/10.1111/j.1468-1331.2009.02862.x.

Nasca, C., Bigio, B., Lee, F.S., Young, S.P., Kautz, M.M., Albright, A., Beasley, J., Millington, D.S., Mathé, A.A., Kocsis, J.H., Murrough, J.W., McEwen, B.S., Rasgon, N., 2018. Acetyl-L-carnitine deficiency in patients with major depressive disorder. Proc. Natl. Acad. Sci. 115, 8627–8632. https://doi.org/10.1073/pnas.1801609115.

Nau, R., Sörgel, F., Eiffert, H., 2010. Penetration of drugs through the blood-cerebrospinal fluid/blood-brain barrier for treatment of central nervous system infections. Clin. Microbiol. Rev. 23, 858–883. https://doi.org/10.1128/CMR.00007-10.

Neale, J.H., Yamamoto, T., 2020. N-acetylaspartylglutamate (NAAG) and glutamate carboxypeptidase II: an abundant peptide neurotransmitter-enzyme system with multiple clinical applications. Prog. Neurobiol. 184, 101722. https://doi.org/10.1016/j.pneurobio.2019.101722.

Ning, X.-A., Liang, J.-Y., Li, R.-J., Hong, Z., Wang, Y.-J., Chang, K.-L., Zhang, Y.-P., Yang, Z.-Y., 2015. Aromatic amine contents, component distributions and risk assessment in sludge from 10 textile-dyeing plants. Chemosphere 134, 367–373. https://doi.org/10.1016/j.chemosphere.2015.05.015.

Noda, T., Kato, R., Ozato, Y., Kawai, Y., Yamamoto, M., Kagawa, Y., Azuma, M., Yamamoto, K., Kusanagi, M., Uryu, K., Harada, H., Ijiri, Y., Hayashi, T., Tanaka, K., 2022. Decreased plasma acetaminophen glucuronide/acetaminophen concentration ratio warns the onset of acetaminophen-induced liver injury. Biopharm. Drug Dispos. 43, 108–116. https://doi.org/10.1002/bdd.2316.

S. Nothias, L.-F., Petras, D., Schmid, R., Dührkop, K., Rainer, J., Sarvepalli, A., Protsyuk, I., Ernst, M., Tsugawa, H., Fleischauer, M., Aicheler, F., Aksenov, A.A., Alka, O., Allard, P.-M., Barsch, A., Cachet, X., Caraballo-Rodriguez, A.M., Da Silva, R.R., Dang, T., Garg, N., Gauglitz, J.M., Gurevich, A., Isaac, G., Jarmusch, A.K., Kameník, Z., Kang, K., Bin, Kessler, N., Koester, I., Korf, A., Le Gouellec, A., Ludwig, M., Martin, H., McCall, C., McSayles, L.-I., Meyer, J., Mohimani, S.W., Morsy, H., Moyne, M., Neumann, O., Neuweger, S., Nguyen, H., Nothias-Esposito, N. H., Paolini, M., Phelan, J., Pluskal, V.V., Quinn, T., Rogers, R.A., Shrestha, B., Tripathi, A., van der Hooft, J.J.J., Vargas, F., Weldon, K.C., Witting, M., Yang, H., Zhang, Z., Zubeil, F., Kohlbacher, O., Böcker, S., Alexandrov, T., Bandeira, N., Wang, M., Dorrestein, P.C., 2020. Feature-based molecular networking in the GNPS analysis environment Nat. Methods 17, 905–908. https://doi.org/10.1038/s41592-020-0933-6.

Obrenovitch, T.P., 2001. Quinolinic acid accumulation during neuroinflammation. Ann. N. Y. Acad. Sci. 939, 1–10. https://doi.org/10.1111/j.1749-6632.2001.tb03605.x.

Ogrinc, K., Hernández, S.A., Korva, M., Bogovič, P., Rojko, T., Lusa, L., Chiumento, G., Strle, F., Strle, K., 2022. Unique clinical, immune, and genetic signature in patients with borrelial meningoradiculoneuritis. Emerg. Infect. Dis. 28, 766–776. https://doi.org/10.3201/eid2804.211831.

Oka, T., Matsuzawa, Y., Tsuneyoshi, M., Nakamura, Y., Aoshima, K., Tsugawa, H., Michael, Weiner, Aisen, P., Petersen, R., Jack, C.R., Jagust, W., 2024. Multiomics analysis to explore blood metabolite biomarkers in an Alzheimer's disease neuroimaging initiative cohort. Sci. Rep. 14, 6797. https://doi.org/10.1038/s41598-024-56837-1.

Othman, A., Rütti, M.F., Ernst, D., Saely, C.H., Rein, P., Drexel, H., Porretta-Serapiglia, C., Lauria, G., Bianchi, R., von Eckardstein, A., Hornemann, T., 2012. Plasma deoxysphingolipids: a novel class of biomarkers for the metabolic syndrome? Diabetologia 55, 421–431. https://doi.org/10.1007/s00125-011-2384-1.

Pang, Z., Lu, Y., Zhou, G., Hui, F., Xu, L., Viau, C., Spigelman, A.F., MacDonald, P.E., Wishart, D.S., Li, S., Xia, J., 2024. MetaboAnalyst 6.0: towards a unified platform for metabolomics data processing, analysis and interpretation. Nucleic Acids Res. 52, W398–W406. https://doi.org/10.1093/nar/gkae253.

Park, J.-M., Kim, M.-J., Noh, J.-Y., Yun, T.G., Kang, M.-J., Lee, S.-G., Yoo, B.C., Pyun, J.-C., 2020. Simultaneous analysis of multiple cancer biomarkers using MALDI-TOF mass spectrometry based on a parylene-matrix chip. J. Am. Soc. Mass Spectrom. 31, 917–926. https://doi.org/10.1021/jasms.9b00102.

Petrick, L.M., Shomron, N., 2022. AI/ML-driven advances in untargeted metabolomics and exposomics for biomedical applications. Cell Rep. Phys. Sci. 3, 100978. https://doi.org/10.1016/j.xcrp.2022.100978.

Pietikäinen, A., Oksi, J., Hytönen, J., 2018. Point-of-care testing for CXCL13 in Lyme neuroborreliosis. Diagn. Microbiol. Infect. Dis. 91, 226–228. https://doi.org/10.1016/j.diagmicrobio.2018.02.013.

Podbielska, M., Ariga, T., Pokryszko-Dragan, A., 2022. Sphingolipid players in multiple sclerosis: their influence on the initiation and course of the disease. Int. J. Mol. Sci. 23, 5330. https://doi.org/10.3390/ijms23105330.

Qu, F., Zhang, H., Zhang, M., Hu, P., 2018. Sphingolipidomic profiling of rat serum by UPLC-Q-TOF-MS: application to rheumatoid arthritis study. Molecules 23, 1324. https://doi.org/10.3390/molecules23061324.

Quehenberger, O., Armando, A.M., Brown, A.H., Milne, S.B., Myers, D.S., Merrill, A.H., Bandyopadhyay, S., Jones, K.N., Kelly, S., Shaner, R.L., Sullards, C.M., Wang, E., Murphy, R.C., Barkley, R.M., Leiker, T.J., Raetz, C.R.H., Guan, Z., Laird, G.M., Six, D. A., Russell, D.W., McDonald, J.G., Subramaniam, S., Fahy, E., Dennis, E.A., 2010. Lipidomics reveals a remarkable diversity of lipids in human plasma. J. Lipid Res. 51, 3299–3305. https://doi.org/10.1194/jlr.M009449.

Ren, J., Yu, L., Lin, J., Liu, Y., Ma, L., huang, Y., Sun, N., Deng, Y., Zhong, D., Zhou, B., Jiang, B., Yan, M., 2025. Elevated 18:1 lysophosphatidylcholine contributes to neuropathic pain in peripheral nerve injury. Reg. Anesth. Pain Med. 0, 1–12. https://doi.org/10.1136/rapm-2024-106195.

Rives, A., Génisson, Y., Faugeroux, V., Saffon, N., Baltas, M., 2009. Enantioselective access to all-trans 5-alkylpiperidine-3,4-diols: application to the asymmetric synthesis of the 1-n-iminosugar (+)-isofagomine. Synthesis (Mass) 19, 3251–3258. https://doi.org/10.1055/s-0029-1216935.

Rousar, T., Handl, J., Capek, J., Nyvltova, P., Rousarova, E., Kubat, M., Smid, L., Vanova, J., Malinak, D., Musilek, K., Cesla, P., 2023. Cysteine conjugates of acetaminophen and p-aminophenol are potent inducers of cellular impairment in human proximal tubular kidney HK-2 cells. Arch. Toxicol. 97, 2943–2954. https://doi.org/10.1007/s00204-023-03569-2.

Rupprecht, T.A., Koedel, U., Fingerle, V., Pfister, H.-W., 2008. The pathogenesis of Lyme neuroborreliosis: from infection to inflammation. Molecular Medicine 14, 205–212. https://doi.org/10.2119/2007-00091.Rupprecht.

Sapon, A., Luhin, V., Sovastei, O., Spanik, P., Bondariev, V., 2017. Identification and fragmentation of cefalosporins, lincosamides, levofloxacin, doxycycline, vancomycin by ESI-MS. Acta Phys. Pol. A 132, 236–239. https://doi.org/10.12693/APhysPolA.132.236.

Schmidt, C., Plate, A., Angele, B., Pfister, H.-W., Wick, M., Koedel, U., Rupprecht, T.A., 2011. A prospective study on the role of CXCL13 in Lyme neuroborreliosis. Neurology 76, 1051–1058. https://doi.org/10.1212/WNL.0b013e318211c39a.

Schwarcz, R., Bruno, J.P., Muchowski, P.J., Wu, H.-Q., 2012. Kynurenines in the mammalian brain: when physiology meets pathology. Nat. Rev. Neurosci. 13, 465–477. https://doi.org/10.1038/nrn3257.

Schymanski, E.L., Jeon, J., Gulde, R., Fenner, K., Ruff, M., Singer, H.P., Hollender, J., 2014. Identifying small molecules via high resolution mass spectrometry: communicating confidence. Environ. Sci. Technol. 48, 2097–2098. https://doi.org/10.1021/es5002105.

Sharma, A., Smith, M.A., Muresanu, D.F., Dey, P.K., Sharma, H.S., 2019. 5-Hydroxytryptophan: a precursor of serotonin influences regional blood-brain barrier breakdown, cerebral blood flow, brain edema formation, and neuropathology. Int. Rev. Neurobiol. 146, 1–44. https://doi.org/10.1016/bs.irn.2019.06.005.

Shi, L., Ghezzi, L., Fenoglio, C., Pietroboni, A.M., Galimberti, D., Pace, F., Hardy, T.A., Piccio, L., Don, A.S., 2025. CSF sphingolipids are correlated with neuroinflammatory cytokines and differentiate neuromyelitis optica spectrum disorder from multiple sclerosis. J. Neurol. Neurosurg. Psychiatry 96, 54–67. https://doi.org/10.1136/jnnp-2024-333774.

Shimizu, Y., Ishikawa, M., Gotoh, M., Fukasawa, K., Yamamoto, S., Iwasa, K., Yoshikawa, K., Murakami-Murofushi, K., 2018. Quantitative determination of cyclic phosphatidic acid and its carba analog in mouse organs and plasma using LC–MS/MS. J. Chromatogr. B 1076, 15–21. https://doi.org/10.1016/j.jchromb.2018.01.002.

Slenter, D.N., Kutmon, M., Hanspers, K., Riutta, A., Windsor, J., Nunes, N., Mélius, J., Cirillo, E., Coort, S.L., Digles, D., Ehrhart, F., Giesbertz, P., Kalafati, M., Martens, M., Miller, R., Nishida, K., Rieswijk, L., Waagmeester, A., Eijssen, L.M.T., Evelo, C.T., Pico, A.R., Willighagen, E.L., 2018. WikiPathways: a multifaceted pathway database bridging metabolomics to other omics research. Nucleic Acids Res. 46, D661–D667. https://doi.org/10.1093/nar/gkx1064.

Smíšková, D., Džupová, O., Moravcová, L., Pícha, D., 2023. Cerebrospinal fluid CXCL13 in non-borrelial central nervous system infections: contribution of CXCL13 to the differential diagnosis. Infect. Dis. 55, 551–558. https://doi.org/10.1080/23744235.2023.2222178.

Stanek, G., Fingerle, V., Hunfeld, K.-P., Jaulhac, B., Kaiser, R., Krause, A., Kristoferitsch, W., O'Connell, S., Ornstein, K., Strle, F., Gray, J., 2011. Lyme borreliosis: clinical case definitions for diagnosis and management in Europe. Clin. Microbiol. Infect. 17, 69–79. https://doi.org/10.1111/j.1469-0691.2010.03175.x.

Steere, A.C., Strle, F., Wormser, G.P., Hu, L.T., Branda, J.A., Hovius, J.W.R., Li, X., Mead, P.S., 2016. Lyme borreliosis. Nat. Rev. Dis. Primers 2, 16090. https://doi.org/10.1038/nrdp.2016.90.

Stoessel, D., Stellmann, J.-P., Willing, A., Behrens, B., Rosenkranz, S.C., Hodecker, S.C., Stürner, K.H., Reinhardt, S., Fleischer, S., Deuschle, C., Maetzler, W., Berg, D., Heesen, C., Walther, D., Schauer, N., Friese, M.A., Pless, O., 2018. Metabolomic profiles for primary progressive multiple sclerosis stratification and disease course monitoring. Front. Hum. Neurosci. 12, 226. https://doi.org/10.3389/fnhum.2018.00226.

Stoffel, W., Dittmar, K., Wilmes, R., 1975. Sphingolipid metabolism in *Bacteroideaceae*. Hoppe. Seylers. Z. Physiol. Chem. 356, 715–726. https://doi.org/10.1515/bchm2.1975.356.s1.715.

Sühs, K.-W., Novoselova, N., Kuhn, M., Seegers, L., Kaever, V., Müller-Vahl, K., Trebst, C., Skripuletz, T., Stangel, M., Pessler, F., 2019. Kynurenine is a cerebrospinal fluid biomarker for bacterial and viral central nervous system infections. J. Infect. Dis. 220, 127–138. https://doi.org/10.1093/infdis/jiz048.

Sumner, L.W., Amberg, A., Barrett, D., Beale, M.H., Beger, R., Daykin, C.A., Fan, T.W.-M., Fiehn, O., Goodacre, R., Griffin, J.L., Hankemeier, T., Hardy, N., Harnly, J., Higashi, R., Kopka, J., Lane, A.N., Lindon, J.C., Marriott, P., Nicholls, A.W., Reily, M. D., Thaden, J.J., Viant, M.R., 2007. Proposed minimum reporting standards for chemical analysis. Metabolomics 3, 211–221. https://doi.org/10.1007/s11306-007-0082-2.

Sun, H., Xing, H., Tian, X., Zhang, X., Yang, J., Wang, P., 2022. UPLC-MS/MS method for simultaneous determination of 14 antimicrobials in human plasma and cerebrospinal fluid: application to therapeutic drug monitoring. J. Anal. Methods Chem. 2022, 7048605. https://doi.org/10.1155/2022/7048605.

Sun, J., Charron, C.S., Liu, Z., Novotny, J.A., Harrington, P., de, B., Ross, S.A., Seifried, H. E., Chen, P., 2020. Study on human urinary metabolic profiles after consumption of kale and daikon radish using a high-resolution mass spectrometry-based non-targeted and targeted metabolomic approach. J. Agric. Food Chem. 68, 14307–14318. https://doi.org/10.1021/acs.jafc.0c05184.

Sun, Y.-J., Zhang, Q.-Y., Liu, F., Chen, L., Wang, J.-F., 2025. Polysaccharides isolated from *Cibotium barometz* attenuate chronic inflammatory pain: molecular chemical structure and role of phenylalanine. Int. J. Biol. Macromol. 297, 139911. https://doi.org/10.1016/j.ijbiomac.2025.139911.

Tokumura, A., Handa, Y., Yoshioka, Y., Higashimoto, M., Tsukatani, H., 1982. Mass spectrometric analyses of lysophosphatidic acids and their dimethyl esters. Chem. Pharm. Bull. 30, 2119–2126. https://doi.org/10.1248/cpb.30.2119.

Tripathy, D., Grammas, P., 2009. Acetaminophen inhibits neuronal inflammation and protects neurons from oxidative stress. J. Neuroinflamm. 6, 10. https://doi.org/10.1186/1742-2094-6-10.

Uchiyama, A., Mukai, M., Fujiwara, Y., Kobayashi, S., Kawai, N., Murofushi, H., Inoue, M., Enoki, S., Tanaka, Y., Niki, T., Kobayashi, T., Tigyi, G., Murakami-Murofushi, K., 2007. Inhibition of transcellular tumor cell migration and metastasis by novel carba-derivatives of cyclic phosphatidic acid. Biochimica et Biophysica Acta (BBA) - Molecular and Cell Biology of Lipids 1771, 103–112. https://doi.org/10.1016/j.bbalip.2006.10.001.

Vallianatou, T., Lin, W., Bèchet, N.B., Correia, M.S., Shanbhag, N.C., Lundgaard, I., Globisch, D., 2021. Differential regulation of oxidative stress, microbiota-derived, and energy metabolites in the mouse brain during sleep. J. Cerebral Blood Flow Metab. 41, 3324–3338. https://doi.org/10.1177/0271678×211033358.

Viljanen, M.K., Punnonen, J., 1989. The effect of storage of antigen-coated polystyrene microwells on the detection of antibodies against *borrelia burgdorferi* by enzyme immunoassay (EIA). J. Immunol. Methods 124, 137–141. https://doi.org/10.1016/0022-1759(89)90195-6.

Waiß, C., Ströbele, B., Graichen, U., Klee, S., Gartlehner, J., Sonntagbauer, E., Hirschbichler, S., Tinchon, A., Kacar, E., Wuchty, B., Novotna, B., Kühn, Z., Sellner, J., Struhal, W., Bancher, C., Schnider, P., Asenbaum-Nan, S., Oberndorfer, S., 2024. CXCL13 as a biomarker in the diagnostics of european Lyme neuroborreliosis - a prospective multicentre study in Austria. J. Cent. Nerv. Syst. Dis. 16, 11795735241247026. https://doi.org/10.1177/11795735241247026.

Wang, J., Zheng, G., Wang, L., Meng, L., Ren, J., Shang, L., Li, D., Bao, Y., 2024. Dysregulation of sphingolipid metabolism in pain. Front. Pharmacol. 15, 1337150. https://doi.org/10.3389/fphar.2024.1337150.

Welbourne, T.C., 1979. Ammonia production and glutamine incorporation into glutathione in the functioning rat kidney. Can. J. Biochem. 57, 233–237. https://doi.org/10.1139/o79-029.

Wepy, J.A., Galligan, J.J., Kingsley, P.J., Xu, S., Goodman, M.C., Tallman, K.A., Rouzer, C.A., Marnett, L.J., 2019. Lysophospholipases cooperate to mediate lipid homeostasis and lysophospholipid signaling. J. Lipid Res. 60, 360–374. https://doi.org/10.1194/jlr.M087890.

Wickström, R., Fowler, Å., Goiny, M., Millischer, V., Ygberg, S., Schwieler, L., 2021. The kynurenine pathway is differentially activated in children with Lyme disease and tick-borne encephalitis. Microorganisms 9, 322. https://doi.org/10.3390/microorganisms9020322.

Wilmore, D.W., Shabert, J.K., 1998. Role of glutamine in immunologic responses. Nutrition 14, 618–626. https://doi.org/10.1016/S0899-9007(98)00009-4.

Wishart, D.S., Guo, A., Oler, E., Wang, F., Anjum, A., Peters, H., Dizon, R., Sayeeda, Z., Tian, S., Lee, B.L., Berjanskii, M., Mah, R., Yamamoto, M., Jovel, J., Torres-Calzada, C., Hiebert-Giesbrecht, M., Lui, V.W., Varshavi, Dorna, Varshavi, Dorsa, Allen, D., Arndt, D., Khetarpal, N., Sivakumaran, A., Harford, K., Sanford, S., Yee, K., Cao, X., Budinski, Z., Liigand, J., Zhang, L., Zheng, J., Mandal, R., Karu, N., Dambrova, M., Schiöth, H.B., Greiner, R., Gautam, V., 2022. HMDB 5.0: the Human Metabolome Database for 2022. Nucleic Acids Res. 50, D622–D631. https://doi.org/10.1093/nar/gkab1062.

Wojciechowska-Koszko, I., Kwiatkowski, P., Sienkiewicz, M., Kowalczyk, M., Kowalczyk, E., Dołęgowska, B., 2022. Cross-reactive results in serological tests for borreliosis in patients with active viral infections. Pathogens 11, 203. https://doi.org/10.3390/pathogens11020203.

Wongchang, T., Winterberg, M., Tarning, J., Sriboonvorakul, N., Muangnoicharoen, S., Blessborn, D., 2022. Determination of ceftriaxone in human plasma using liquid chromatography–tandem mass spectrometry. Wellcome Open Res. 4, 47. https://doi.org/10.12688/wellcomeopenres.15141.3.

Wu, D., Li, X., Zhang, X., Han, F., Lu, X., Liu, L., Zhang, J., Dong, M., Yang, H., Li, H., 2020a. Pharmacometabolomics identifies 3-hydroxyadipic acid, D-galactose, lysophosphatidylcholine (P-16:0), and tetradecenoyl-L-carnitine as potential predictive indicators of gemcitabine efficacy in pancreatic cancer patients. Front. Oncol. 9, 1524. https://doi.org/10.3389/fonc.2019.01524.

Wu, H., Wang, L., Zhan, X., Wang, B., Wu, J., Zhou, A., 2020b. A UPLC-Q-TOF/MS-based plasma metabolomics approach reveals the mechanism of Compound Kushen injection-based intervention against non-small cell lung cancer in Lewis tumor-bearing mice. Phytomedicine 76, 153259. https://doi.org/10.1016/j.phymed.2020.153259.

Wu, N., Yang, M., Gaur, U., Xu, H., Yao, Y., Li, D., 2016. Alpha-ketoglutarate: physiological functions and applications. Biomol. Ther. 24, 1–8. https://doi.org/10.4062/biomolther.2015.078.

Xue, A., Zhao, D., Xu, H., Lei, X., Li, D., Ren, Y., Zhou, Q., Qiu, Q., Cai, L., Zhang, Y., Zhang, N., 2025. Erzhi pill promotes norepinephrine synthesis in locus coeruleus through ERβ-TFAP2A-TH plays a neuroprotective role. J. Ethnopharmacol. 350, 120015. https://doi.org/10.1016/j.jep.2025.120015.

Yan, X., Li, P., Liu, C., Yin, F., Han, J., Sun, H., Zheng, Y., Chen, X., Guan, S., Wang, X., 2025. Exploring the molecular mechanisms for renoprotective effects of Huangkui capsule on diabetic nephropathy mice by comprehensive serum metabolomics analysis. J. Ethnopharmacol. 340, 119223. https://doi.org/10.1016/j.jep.2024.119223.

Yang, Y., Chen, Z., Yan, G., Kong, L., Yang, L., Sun, H., Han, Y., Zhang, J., Wang, X., 2023. Mass spectrum oriented metabolomics for evaluating the efficacy and discovering the metabolic mechanism of Naoling Pian for insomnia. J. Pharm. Biomed. Anal. 236, 115756. https://doi.org/10.1016/j.jpba.2023.115756.

Zhang, J., Li, Z., Zhang, Y., Guo, Y., Zhu, Y., Xia, W., Dai, Y., Xia, Y., 2023a. Mume fructus (Prunus mume Sieb. et Zucc.) extract accelerates colonic mucosal healing of mice with colitis induced by dextran sulfate sodium through potentiation of cPLA2-mediated lysophosphatidylcholine synthesis. Phytomedicine 119, 154985. https://doi.org/10.1016/j.phymed.2023.154985.

Zhang, X., Li, R., Hu, W., Zeng, J., Jiang, X., Wang, L., 2018. A reliable LC-MS/MS method for the quantification of *N*-acetyl-*p*-benzoquinoneimine, acetaminophen glutathione and acetaminophen glucuronide in mouse plasma, liver and kidney: method validation and application to a pharmacokinetic study. Biomed. Chromatogr. 32, e4331. https://doi.org/10.1002/bmc.4331.

Zhang, X.-Y., Xu, J.-D., Wang, Y., Wu, C.-Y., Zhou, J., Shen, H., Zou, Y.-T., Zhu, J.-H., Zhou, S.-S., Li, S.-L., Xu, J., Long, F., 2023b. Comparing steamed and wine-stewed Rehmanniae Radix in terms of yin-nourishing effects via metabolomics and microbiome analysis. J. Ethnopharmacol. 311, 116424. https://doi.org/10.1016/j.jep.2023.116424.

Zhang, Z.-T., Qi, Y., Chen, P., Chen, L., Jiang, Y., Fan, Z., Guan, H., Bai, L., Liu, J., Zhao, D., Yan, G., 2024. Dang-Gui-Bu-Xue decoction against diabetic nephropathy via modulating the carbonyl compounds metabolic profile and AGEs/RAGE pathway. Phytomedicine 135, 156104. https://doi.org/10.1016/j.phymed.2024.156104.

Zhao, H., Zhang, Y., Liu, B., Zhang, L., Bao, M., Li, L., Zhao, N., Hussain, M., Wang, Y., Yi, J., Chen, P., Lu, C., 2020. A pilot study to identify the longitudinal serum metabolite profiles to predict the development of hyperuricemia in essential hypertension. Clinica Chimica Acta 510, 466–474. https://doi.org/10.1016/j.cca.2020.08.002.